AFRL-VS-TR-2002-1529

Algorithms and Preliminary Experiences with the LN93 and LN100 for Airborne Vector Gravimetry

Christopher Jekeli

Department of Civil Engineering and
Geodetic Science
Ohio State University
2070 Neil Ave
Columbus, OH 43210

August 1998

AIR FORCE RESEARCH LABORATORY
Space Vehicles Directorate
29 Randolph Rd
AIR FORCE MATERIEL COMMAND
HANSCOM AFB, MA 01731-3010

This technical report has been reviewed and is approved for publication

(Signature)
David M. Gleason
Contract Manager

(Signature)
Mark P. Wilson, Major, USAF
Space Weather Effects Team Lead

(Signature)
Gregory P. Ginet, Chief
Space Weather Center of Excellence

This report has been reviewed by the ESC Public Affaires Office (PA) and is releasable to the National Technical Information Service (NTIS).

Qualified requestors may obtain additional copies from the Defense Technical Information Center (DTIC). All others should apply to the National Technical Information Service (NTIS).

If your address has changed, if you wish to be removed from the mailing list, or if the addressee is no longer employed by your organization, please notify AFRL/VSIM, 29 Randolph Road, Hanscom AFB, MA 01731-3010. This will assist us in maintaining a current mailing list.

Do not return copies of this report unless contractual obligations or notices on a specific document require that it be returned.

REPORT DOCUMENTATION PAGE	Form Approved OMB No. 0704-0188

1. AGENCY USE ONLY *(Leave blank)*	2. REPORT DATE	3. REPORT TYPE AND DATES COVERED
	August 1998	Scientific, Final, 12 Sep 1995-5 Jul 1998

4. TITLE AND SUBTITLE
Algorithmns and Preliminary Experiences with the LN93 and LN100 for Airborne Vector Gravimetry

5. FUNDING NUMBERS
Contract F19628-95-K-0020
PE 663200
PR DMAP
TA GL
WU AB

6. AUTHOR(S)
Christopher Jekeli

7. PERFORMING ORGANIZATION NAME(S) AND ADDRESS(ES)
Ohio State University Research Foundation
1960 Kenny Rd
Columbus, OH 43210-1063

8. PERFORMING ORGANIZATION REPORT NUMBER

9. SPONSORING/MONITORING AGENCY NAME(S) AND ADDRESS(ES)
Air Force Research Laboratory
29 Randolph Rd
Hanscom AFB, MA 01731-3010
Contract Manager: David Gleason/VSBXT

10. SPONSORING/MONITORING AGENCY REPORT NUMBER
AFRL-VS-TR-2002-1529

11. SUPPLEMENTARY NOTES

12a. DISTRIBUTION AVAILABILITY STATEMENT
Approved for Public Release; distribution unlimited

12b. DISTRIBUTION CODE

13. ABSTRACT *(Maximum 200 words)*

This report presents the results of investigations in using a medium-to-high accuracy inertial naviagation system (INS_) and a geodetic quality Global Positioning System (GPS) receiver on an airborne platform to determine the gravity disturbance vector along the trajectory of an aircraft. The main products of these investigations consist of derivations of alternative algorithms to estimate the horizontal gravity vector components given that the INS's under consideration have diferent types of available output data, either time-integrated accelerations and direction cosines or raw accelerometer and gyro data. In addition, two distinct data processing methodologies are elucidated to combine the GPS and INS data. The first is based on a traditional Kalman filter approach that treats the gravity disturbance vector as a stochastic process, and the second is an extension of the scalar airborne gravimetry concept. also, the configuration details of a loosely coupled INS/GPS sysem for airborne application are given, with particular emphasis on time synchronization.

A limited number of field tests (ground and airborne) with the LN93 and LN100 were performed. Results from these tests verity the specified accuracy of the INS and yield initial attempted estimations of the vertical deflection using the Kalman filter approach. While the latter are inconclusive in assessing the precision level achievable with this method and instrumentation (due to unexpectedly poor gyro performance), they do indicate the feasibility of the approach provided the INS gyros perform at the specified level.

14. SUBJECT TERMS
Gravimetry Gradiometry Vertical Inertial navigation

15. NUMBER OF PAGES

16. PRICE CODE

17. SECURITY CLASSIFICATION OF REPORT	18. SECURITY CLASSIFICATION OF THIS PAGE	19. SECURITY CLASSIFICATION OF ABSTRACT	20. LIMITATION OF ABSTRACT
UNCL	UNCL	UNCL	UNL

Abstract

This report presents the results of investigations in using a medium-to-high accuracy inertial navigation system (INS) and a geodetic quality Global Positioning System (GPS) receiver on an airborne platform to determine the gravity disturbance vector along the trajectory of the aircraft. The main products of these investigations consist of derivations of alternative algorithms to estimate the horizontal gravity vector components given that the INS's under consideration have different types of available output data, either time-integrated accelerations and direction cosines or raw accelerometer and gyro data. In addition, two distinct data processing methodologies are elucidated to combine the GPS and INS data. The first is based on a traditional Kalman filter approach that treats the gravity disturbance vector as a stochastic process, and the second is an extension of the scalar airborne gravimetry concept. Also, the configuration details of a loosely coupled INS/GPS system for airborne application are given, with particular emphasis on time synchronization.

A limited number of field tests (ground and airborne) with the LN93 and LN100 were performed. Results from these tests verify the specified accuracy of the INS and yield initial attempted estimations of the vertical deflection using the traditional Kalman filter approach. While the latter are inconclusive in assessing the precision level achievable with this method and instrumentation (due to unexpectedly poor gyro performance), they do indicate the feasibility of the approach provided the INS gyros perform at the specified level.

1 Background

Knowledge of the Earth's gravity field is an essential element in most geodetic and many geophysical applications, dating back to the 17th century (Newton, Huygens), and firmly established for geodesy by F.R. Helmert (1880) who developed the modern concept of the *geoid* as geodetic reference surface to approximate the shape of the Earth. (The geoid is an equipotential surface of the Earth's gravity field that closely approximates mean sea level.) Since the 1950's, the Earth's gravitational field also played a significant role in satellite orbit determination and in inertial navigation and guidance. Conversely, with observations of satellite orbits, and especially with satellite altimetry over the oceans (approximately the geoid), as well as the steady accumulation of surface gravity measurements, very accurate models of the Earth's gravity field have been developed during the last forty years, and significant strides have been made during the last decade (Nerem, 1995; Nerem et al., 1995). With these efforts, the geoid can now be calculated worldwide to an accuracy of better than one meter (NIMA, 1997); in ocean areas to about 30 cm (Rapp, 1996), and on some continents to better than 2 cm over 50 km (Milbert, 1997; see also Balmino and Sanso, 1995). Yet the gravity field with its infinite detail and information remains a key component in geodesy and geophysics and the object of continually improving measurement.

One particularly relevant need to know the Earth's gravity field concerns inertial navigation and guidance systems. Historically, the inertial navigation system (INS) has provided the principal means of autonomous navigation and guidance systems of aircraft, ships (including submarines), and missiles. The recent rapid developments and achievement of high accuracy with the Global Positioning System (GPS) have quickly overtaken the INS in terms of the range of applications and the long-term maintenance of mission accuracy. However, due to the recognition of the limitations and vulnerabilities of GPS, as well as new technological advancements in inertial instrumentation, INS is considered a valuable, if not indispensable means to enhance, aid, or replace GPS in various navigation, positioning, and guidance scenarios. Inertial navigation still is the only method that provides fully autonomous, completely stealthy, and jam-proof navigation and guidance. Efforts to make GPS immune to jamming have been largely unsuccessful.

On the other hand, unlike GPS, very precise inertial navigation systems require knowledge of the Earth's local gravity vector field, specifically the direction of the gravity vector. It may be noted that GPS also requires some knowledge of the Earth gravitational field in order to determine precise orbits of the GPS satellites; however, only very long-wavelength information is required since the orbits have high altitude (20,000 km). The direction of gravity is prescribed naturally by

the total mass density structure of the Earth and can be referenced to the direction defined by the surface normal (perpendicular) of a rotational ellipsoid that approximates the geoid. The difference between these two directions is known as the deflection of the vertical. The two angular components of the deflection of the vertical are also related directly to the horizontal (with respect to the ellipsoid) components of the gravity vector (Figure 1), where the signs are a matter of convention.

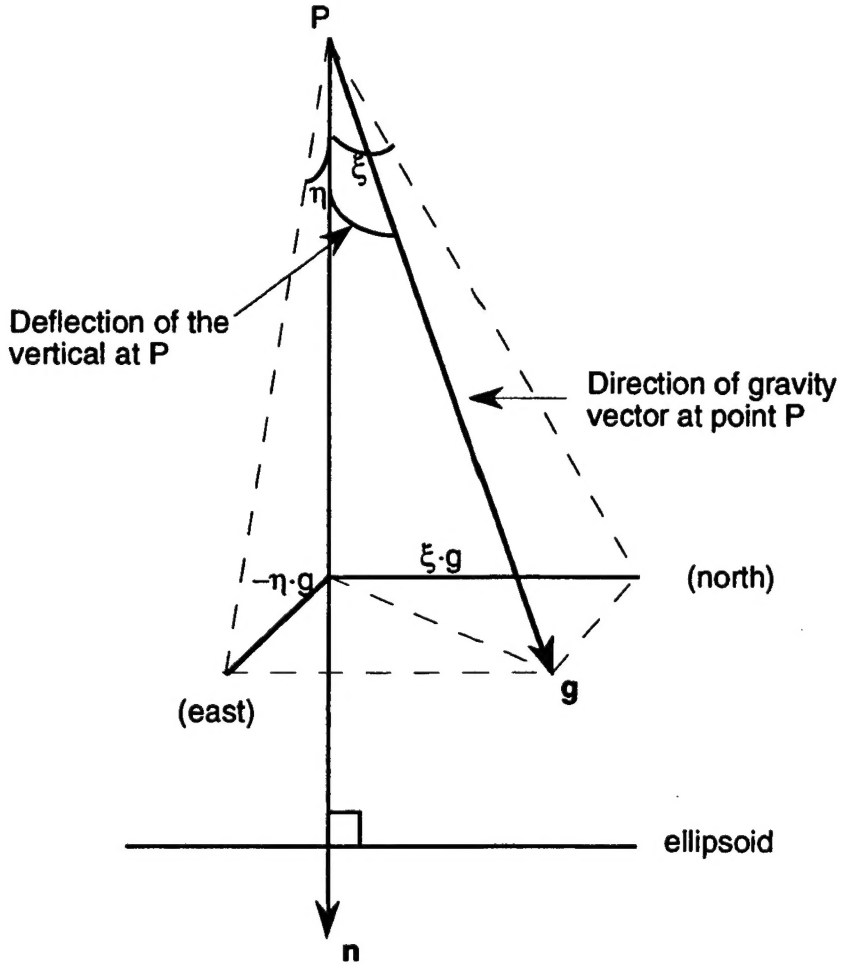

Figure 1: The geometry of the deflection of the vertical.

Although global models for the Earth's gravitational field are improving (like NIMA's EGM96, Lemoine (1996)) shorter-wavelength signatures are either very poorly modeled (less than 100 km) or only moderately well known (100 km to 1000 km), especially in rugged terrain regions of the world and the polar regions. A recent study by Jekeli (1998a), that compares astronomically determined deflections of the vertical in the United States to corresponding deflections computed from EGM96, indicates that the EGM96 gravity model at wavelengths shorter than 200 km may be

under-powered. This conclusion (requiring further verification) is indicated from considerations of the implied power of the signal beyond the cutoff wavelength of 100 km. Specifically, the EGM96 model implies that the root-mean-square of the deflection of the vertical with wavelengths shorter than 100 km in the conterminous U.S. (CONUS) is only 1.33 arcsec; while the corresponding value for the astronomically determined deflections in CONUS is 3.84 arcsec.

On the other hand, a significant part of the error budget of high accuracy inertial systems (0.1 to 1.0 nmi/hr systems) is the unknown gravity field, as shown by Jekeli (1997). That is, a high accuracy system which should be accurate to 0.1 nautical mile per hour (or, assuming linearity, about 15 meters per 5 minutes) is susceptible to unknown gravity effects (even with respect to EGM96) of about 10 meters over that same interval. Also, it is seen in this study that gravity compensation for high-accuracy INS is required primarily for wavelengths greater than 10 km, or higher depending on the speed of the vehicle. Therefore, better knowledge of the Earth's gravity field, especially at wavelengths between 10 km and 200 km, is required to support high accuracy (free-) inertial worldwide navigation and guidance.

Lacking accurate and sufficiently dense (vertical) gravity surveys, the total gravity vector is still not well known in remote and inaccessible regions, such as the Himalayas, the Andes, the polar regions, some coastal regions, and some interior continental regions. To support improved modeling of the gravity vector field requires regional gravity mapping. The more direct method using astronomic measurements to determine the direction of gravity is considered too costly, as well as practically unfeasible, in many regions. However, it is possible to estimate, on the basis of potential theory, the horizontal gravity components from vertical component values that are densely distributed regionally. Therefore, to date, most determinations of the deflections have been derived from scalar (vertical) gravimetry. That is, only the vertical component of the gravity vector is measured since this is much easier in terms of methodology and cost. These surveys can be done on the ground using conventional gravimetric surveys or with much greater efficiency and accessibility to remote areas, but with less accuracy, using airborne platforms. For example, one of the most successful of the airborne gravimetric systems is being operated by the Naval Research Laboratory (NRL) by Dr. John Brozena (Brozena and Peters, 1994). Recently, vast previously unmapped areas of Greenland and the Arctic Ocean were overflown with a gridded pattern by NRL yielding an accuracy of about 5 mgal with 15 km resolution in the vertical gravity values (Forsberg and Kenyon, 1994).

A significant drawback of scalar surveys is that the determination of the horizontal gravity components requires numerical integration of gravity data over larger regions (Vening-Meinesz integrals). Thus, mapping the total gravity vector using scalar gravimetry relies not only on accurate measurements over large regions, but also on a physical model (usually approximate) that

relates the measurements to the desired quantities, in this case, horizontal gravity components.

Other moving-base systems that measure the total gravity vector or the gravity gradient tensor have been considered (and tested, in the case of the gradiometer, Jekeli (1988)). These systems provide a more direct (in situ) measure of the vector field and rely less on the use of approximate potential theory models to estimate the deflection components. A fully operational system, the Gravity Gradiometer Survey System (GGSS) constructed by Bell Aerospace, was tested under NIMA (formerly DMA) sponsorship in the 1980's and yielded 3-6 mgal accuracy of wavelengths between 10 and 100 km in the horizontal components of the gravity vector (Jekeli, 1993). This particular gravity gradiometer system measures the five independent gravity gradients that can be integrated to yield the gravity vector. The gradiometer is considered in the geophysical community to be the instrument that will yield the high resolution and accuracy (1 mgal over 1 km) gravity surveys needed for mineral exploration, upper crustal structure modeling, and local geoid determination. Therefore, gravity gradiometry promises to yield directly the fine structure of the vector gravity field, while also overcoming the scalar limitations. Further development of instruments and testing are needed to demonstrate the full potential of these systems.

A third system that has been under study for some time, but not fully realized in practice, is the integrated INS/GPS platform. The principle of measurement is identical to moving-base scalar gravimetry, but extended to three dimensions. With GPS one measures the total kinematic three-dimensional acceleration of the vehicle as determined from its three-dimensional positions. Using the triad of accelerometers in the INS one measures the three-dimensional specific forces acting on the vehicle. The difference between the two types of acceleration vectors is the gravitational vector. As such, the INS/GPS system provides direct measurements of the horizontal (and vertical) gravity components that rely only on the quality of the measurement systems and not on (usually approximate) analytic models relating vertical and horizontal components. On the other hand, the quality of the sub-systems, INS and GPS, is such that errors at both ends of the spectrum limit the gravitational signal that may be extracted from such an integration. Nevertheless, numerous studies have been conducted that show the feasibility of integrating INS with GPS to conduct airborne vector gravimetry (Eissfeller and Spietz, 1989; Schwarz et al., 1992; Jekeli, 1995). Simulation studies by Jekeli (1995), Gleason (1992), and Wang et al. (1997), among others, have shown that the accuracy of recoverable gravity is about 3-4 mgal over wavelengths of 30 km to 200 km using a high-accuracy INS and differential GPS positioning. The development of such systems has been hindered in part by the expense of high quality INS, being about five times the cost of a high quality GPS receiver.

The most difficult aspect of vector gravimetry using GPS/INS is the drift error in the angular data provided by the gyros that are needed to properly orient the accelerometers. An orientation

error at the level of 1 arcsec translates into a 5 mgal error in the horizontal gravity component. The growth in the orientation error can be controlled by imposing velocity control (zero velocity updates, or ZUPT's) at frequent intervals (e.g., Rose and Nash, 1972); or on an airborne system by using a star tracker to provide absolute orientation of the system to an external reference frame, as was done with success by Northrop Corporation (1986). Alternative, less costly schemes have been considered, such as photogrammetric control (Wang et al., 1997). Or, Jekeli (1995) also argued that if the orientation error growth is indeed a long wavelength phenomenon, then short-wavelength gravity estimation should be possible without resorting to external attitude aiding, where the long-wavelength component ($\geq$ 200 km) would come from a global spherical harmonic model.

This report reviews some of the activities surrounding the use of the LN93 and LN100 Litton inertial navigation systems and the Global Positioning System (GPS) to measure the total gravity vector using an airborne platform. No conclusive results from actual test flight can be reported at this time; however, various models and evaluations of the INS are presented, with recommendations for further studies.

2 INS Instrumentation and Measurements

An inertial navigation system (INS) consists of an inertial measurement unit (IMU) and a navigation computer. The essential element of an IMU is the accelerometer whose output is integrated twice in time to obtain positions. A common class of accelerometers is the force-rebalance type. Although a variety of designs exist, most are based on the principle of maintaining the null position of a proof mass on a spring. The electronically applied force needed to do this is a measure of the acceleration. Three accelerometers with sensitive axes mutually perpendicular provide three-dimensional navigation.

Of equal importance, however, is the coordinate frame in which the accelerometers are to provide positions. In this respect, not only the orientation of the accelerometers in the coordinate system, but also their angular velocity affect the determination of position. The orientation determines the component of the position vector that a particular accelerometer provides; and, as is known from elementary physics, the angular rates with respect to an inertial frame contaminate the accelerometer outputs with centrifugal and Coriolis accelerations.

The orientation and angular rates of the accelerometer platform are determined with gyroscopes. Most INS for commercial deployment, today, use either the *ring laser gyro* or the less costly (and less accurate) *fiber optic gyro*. Both types of gyros require that the INS be

mechanized in the so-called *strapdown* configuration; that is the INS is physically mounted to the frame of the vehicle (no gimbal support system). This reduces the cost of the INS considerably as compared to gimbal-supported, local-level stabilized systems. It also subjects the system to the entire spectrum of vehicle dynamics and the navigation accuracy is less than with the stabilized (motion-isolated) systems. Figure 2 is a schematic drawing of a strapdown platform for the IMU's.

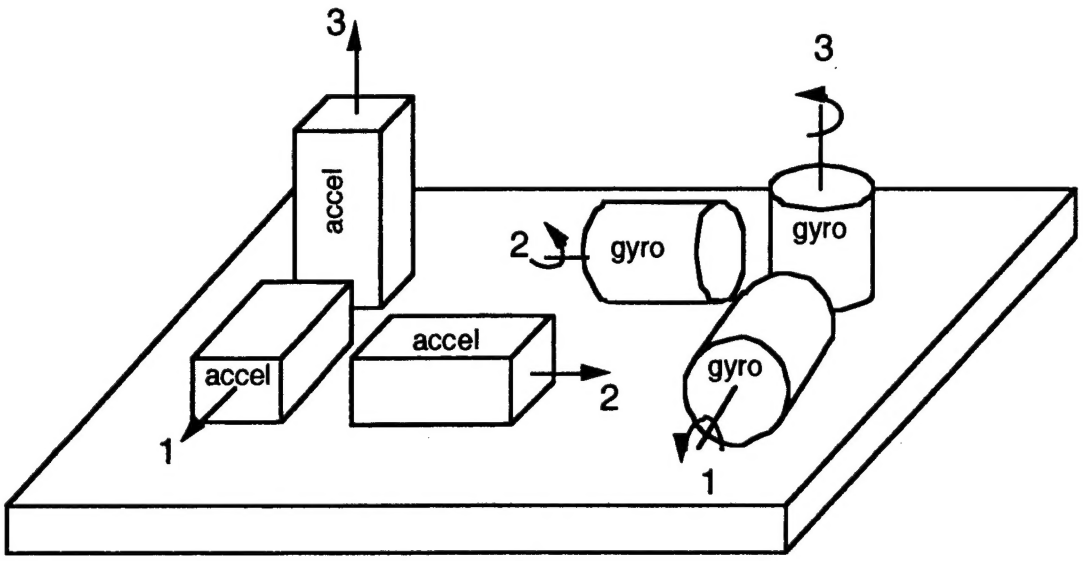

Figure 2. Inertial Measurement Units in a strapdown system.

The ring laser gyro (RLG), in principle, has no moving parts – it is based on the fact that the frequency of a light beam travelling in a resonant closed circuitous path (where the number of wavelengths is always the same; i.e., it is a laser) must change if the *apparent* length of the circuit changes because it rotates in inertial space. The latter property is called the Sagnac effect and is a consequence of general relativity where the speed of light is a constant independent of the frame in which it is traveling. Two such counter-travelling beams of light are used to create a fringe pattern where they recombine. The fringe pattern is stationary if there is no rotation in inertial space. But, it migrates in the presence of rotation about the axis perpendicular to the plane of the circuit, because then one beam sees a longer path, the other a shorter path; and the number of fringes passing a detector per unit time indicates the rate of rotation.

The major problem with RLG's is a phenomenon called lock-in: due to imperfections (scattering of light in the resonant cavity) the two beams lase at the same frequency even in the presence of a small rotation, typically up to several hundred degrees per hour. They lock to the same frequency and indicate a zero rotation. One common solution to this problem is to bias the

output of the device by applying a physical rotation away from the lock-in range. To maintain stability, this mechanical "bias" is in the form of an alternating rotation, i.e., a dithering or oscillation (tens to hundreds of Hz) of the gyro about its sensitive axis. This is the operational concept of the gyros used in the Litton LN93 INS.

A newer approach is to apply an optical bias by creating left- and right-circular polarization of the two beams, respectively. In the presence of an applied magnetic field, the speeds of the beams differ, which is equivalent to an effective difference in path length (Faraday effect), hence creating a bias in the frequency difference. The complete absence of moving parts (no mechanical dithering) improves the stability and substantially reduces the random noise of the IMU as a whole. This is the operational concept of the gyros used in the Litton LN100 INS.

Size, weight, and power requirements, as well as the standard error budgets for each system are listed in Table 1 and Table 2. The accelerometers are the same model for both systems, but presently manufactured sensors are slightly improved. The characteristics of these two systems were provided by Litton (person communication). Both are quite similar and several other subordinate error sources, especially misalignments, temperature transients, and other correlated noise, as well as acceleration sensitivities are not included here.

Table 1: Essential characteristics of the LN93 and LN100 inertial systems.

	LN93	LN100
Data Rate	20 Hz (user defined)	32 Hz (256 Hz, raw data)
Size (excludes mount)	1089 cu. in.	539 cu. in.
Weight (excludes mount)	48.5 lbs.	19.4 lbs
Power	28 VDC, 150 Watts	28 VDC, 26.5 Watts

Table 2: Essential error budget for LN93 and LN100 inertial systems.

	LN93	LN100
Accelerometer (Litton A-4 model)		
Bias Error	25 mGal	20 mGal
Scale Factor Error	120 ppm	40 ppm
White Noise	5 mGal/√Hz	5 mGal/√Hz
Gyro (ring laser gyro)		
Bias (Drift) Error	0.003 °/hr	0.003 °/hr
Scale Factor Error	5 ppm	0.2 ppm
White Noise	0.0015 °/√hr	< 0.001 °/√hr

Figure 3 shows the basic configuration of the INS and computer interface for the LN93. A similar setup exists for the LN100. The computer used with the LN93 is a laptop computer mounted in a so-called docking station that contains both the 1553 bus controller card and the timer card. The 1553 card is the direct interface to the INS and all requests of data from the INS are made through this bus controller. The timer card can be programmed to synthesize a sequence of interrupts at a specified rate which is then used to request the INS data at that rate. In the case of the LN93, the data request rate is 20 Hz. All INS data requests are synchronized to GPS time. Each data item from the INS includes a time tag relative to the INS clock which can be used to determine the actual time for which the data item corresponds. Additional data are retrieved from the GPS receiver by the bus controller software to determined the actual GPS time stamp of the one-second-pulse, and to provide altitude data for the INS. The INS data are saved by the bus controller software in the RAM of the laptop computer and transferred to hard disk storage at the conclusion of the mission. The GPS raw data are stored in the GPS receiver and also later retrieved and processed.

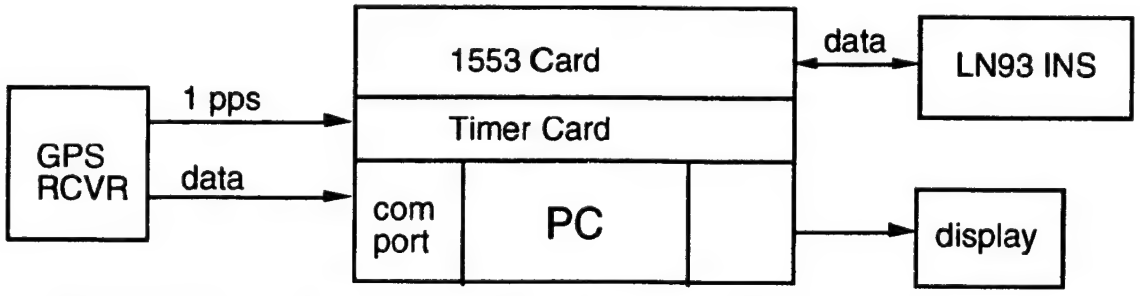

Figure 3: Basic configuration of INS, GPS receiver, and computer test equipment.

The data output options of an INS range from position and velocity to orientation angles, as well as raw sensor data, system status data, and time tags. The type of output is entirely dictated by the navigation software that the INS manufacturer creates for its customers. The software for the LN93, that is on loan to Ohio State University from Litton, allows users to request position and velocity in the navigation frame (wander-azimuth frame) and the navigation-frame-to-Earth-fixed-frame direction cosine matrix, all with double precision (32 bit data), while orientation angles of the body frame with respect to the navigation frame are available only in single precision (16 bit data). No raw accelerometer and gyro data are available. The position coordinates have quantization errors of about 43 cm in latitude and 63 cm in longitude, being due entirely to an artifact of the data processing performed by the navigation software. This is shown in Figure 4 where differences between indicated latitude and longitude values (converted to linear measures in units of meters) where computed for one-second intervals. The data were obtained by moving the LN93 in the laboratory. The velocities do not have this quantization error and can be integrated independent of the INS software to obtain position coordinates at a precision level of a centimeter, or better.

Nevertheless, the lack of availability of raw sensor data from the LN93 makes it less useful for wider geodetic applications and tightly coupled integration with GPS. In addition, care must be exercised in synchronizing the INS and GPS data, since the INS software, performing real-time data processing, makes data available to the user with time validity tags showing significant time delays from the actual data output time. The software of the LN100 obtained by OSU's Center for Mapping was specifically modified to provide raw sensor data which can be processed by the user independently of the navigation software. Furthermore, the time synchronization is less problematic since the time of raw sensor output coincides very closely to the time validity of the data (since very little processing takes place in the INS). The raw data for the LN100 consist of velocity increments from the accelerometers and angle increments from the gyros at the high sampling rate of 256 Hz. In Section 3, algorithms are developed to process these data for geodetic applications.

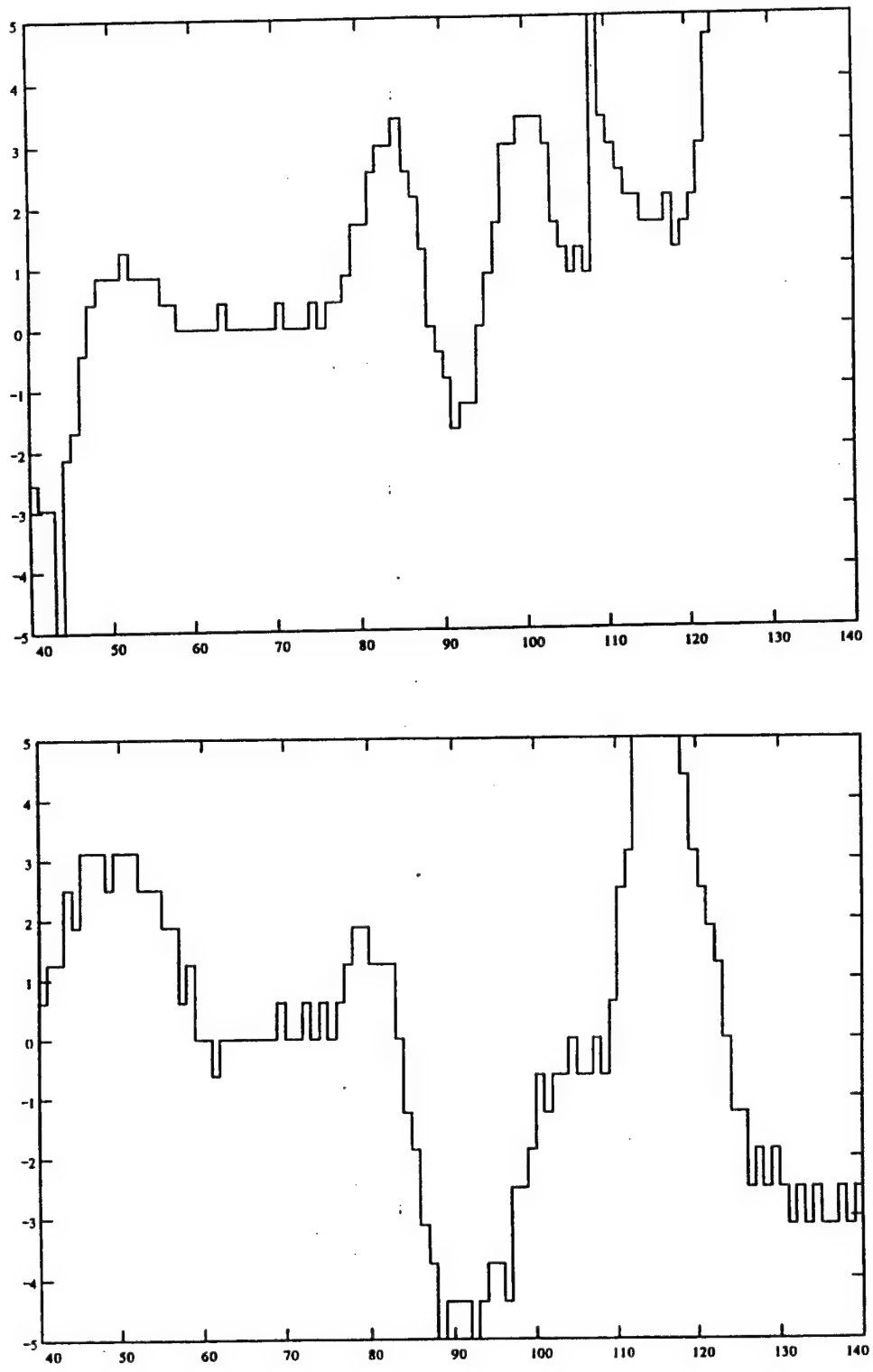

Figure 4. LN93 indicated latitude differences (top) and longitude differences (bottom) between 1-second epochs. Ordinate is in units of meters; abscissa in units of seconds.

3 Algorithms and Models for Vector Gravimetry

3.1 Basic Equations

Navigation using an INS requires knowledge of the Earth's gravity vector field. That is, the INS operates under the basic relationship (Newton's Second Law of Motion) between specific force sensed by accelerometers, $\mathbf{a}$, and total acceleration of the vehicle, the second time derivative of position, $\ddot{\mathbf{x}}$, given by:

$$\ddot{\mathbf{x}} = \mathbf{a} + \mathbf{g} \tag{1}$$

where $\mathbf{g}$ is the gravitation vector. Integrating this equation to get position, $\mathbf{x}$, and velocity, $\dot{\mathbf{x}}$, from sensed acceleration, $\mathbf{a}$, requires knowledge of the gravitation vector, $\mathbf{g}$. Conversely, combining INS with an independent measurement of $\mathbf{x}$ (or $\ddot{\mathbf{x}}$), such as from GPS, yields a measurement of $\mathbf{g}$.

Equation (1) holds for an inertial frame, only. For frames attached to the rotating Earth, or to a vehicle, similar equations are readily derived, but are complicated by the inclusion of Coriolis terms arising from the rotation of the Earth or vehicle with respect to an inertial frame (see Britting, 1971; Jekeli, 1998b). Usually, for local-level mechanizations, the gravitation vector is combined with the centrifugal acceleration arising from Earth's rotation and is then called the *gravity vector*. For the sake of simplicity we use the notation, $\mathbf{g}$, for the gravity vector, as well, since the gravitation vector will not reappear in our discussions. The gravity vector may be separated into two parts, a dominant, so-called *normal gravity* vector, $\boldsymbol{\gamma}$, that accounts for the centrifugal part and all but about one part in 10^4 of the total gravitational vector, and a residual, the so-called *disturbance gravity vector*, $\delta\mathbf{g}$, such that $\mathbf{g} = \boldsymbol{\gamma}\,\mathbf{n} + \delta\mathbf{g}$, where $\mathbf{n}$ is a unit vector along the normal to an ellipsoid and $\gamma = |\boldsymbol{\gamma}|$. The value γ can be calculated exactly on the basis of a well defined normal gravity field (Heiskanen and Moritz, 1967), where for highest accuracy at points above the ellipsoid, the curvature of the field's horizontal gradient must be taken into account. In a local north-east-down coordinate system

$$\delta\mathbf{g} = \mathbf{g} - \boldsymbol{\gamma} = \begin{pmatrix} g\,\xi & -g\,\eta & \delta g \end{pmatrix}^T \tag{2}$$

(see Figure 1) where ξ, η are the deflection of the vertical components, and $\delta g = |\mathbf{g}| - \gamma$ is the (scalar) *gravity disturbance*.

The analogue to equation (1), now formulated for the north-east-down coordinate frame, is

written as

$$\frac{d}{dt}\mathbf{v}^n = \mathbf{a}^n - \left(\boldsymbol{\omega}_{in}^n + \boldsymbol{\omega}_{ie}^n\right) \times \mathbf{v}^n + \mathbf{g}^n \tag{3}$$

where $\mathbf{v}^n$ is the velocity in the navigation frame (n-frame); $\mathbf{a}^n$ and $\mathbf{g}^n$ are, respectively, the sensed acceleration and gravity vector, both coordinatized in the n-frame; and $\boldsymbol{\omega}_{in}^n$, $\boldsymbol{\omega}_{ie}^n$ are angular rate vectors, respectively, of the n-frame and of the Earth-fixed frame (e-frame) each with respect to the inertial frame (i-frame), as coordinatized in the n-frame (Britting, 1971). The second term on the right of (3) is essentially due to the Coriolis and centrifugal accelerations of the n-frame with respect to the i-frame.

The LN93 navigation software uses the so-called wander-azimuth frame to perform the integration of the navigation equations. This avoids certain singularities in the navigation equations near the polar regions where the meridians converge (and longitude rate becomes undefined). The wander azimuth frame is related to the n-frame as shown in Figure 5. The navigation equations in this case are given by

$$\frac{d}{dt}\mathbf{v}^w = \mathbf{a}^w - \left(\boldsymbol{\omega}_{iw}^w + \boldsymbol{\omega}_{ie}^w\right) \times \mathbf{v}^w + \mathbf{g}^w \tag{4}$$

where $\mathbf{v}^w$ is the velocity in the w-frame, and $\mathbf{a}^w$, $\mathbf{g}^w$ similarly are coordinatized in the w-frame. The sum of angular rate vectors in (4) is also equal to

$$\begin{aligned} \boldsymbol{\omega}_{iw}^w + \boldsymbol{\omega}_{ie}^w &= \boldsymbol{\omega}_{ie}^w + \boldsymbol{\omega}_{ew}^w + \boldsymbol{\omega}_{ie}^w \\ &= \boldsymbol{\omega}_{ew}^w + 2\, C_e^w\, \boldsymbol{\omega}_{ie}^e \end{aligned} \tag{5}$$

where C_e^w is the transformation matrix from the e-frame to the w-frame. It is determined by integrating the angular rates, $\boldsymbol{\omega}_{ew}^w$, given approximately by

$$\boldsymbol{\omega}_{ew}^w \approx \frac{1}{r}\begin{pmatrix} v_2^w \\ -v_1^w \\ 0 \end{pmatrix} \tag{6}$$

where r is the geocentric radius to the vehicle. The details of this integration are analogous to the procedure outlined below for the raw gyro data processing.

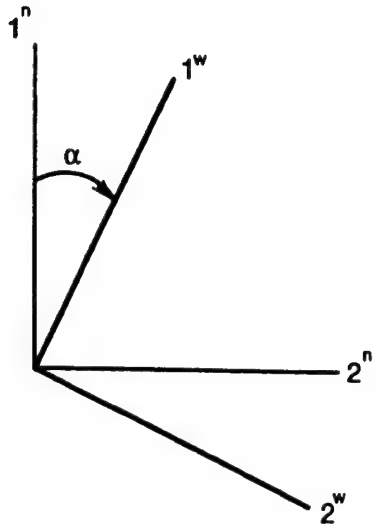

Figure 5: Wander-azimuth frame

As a first approximation, navigation computers use only the readily computable normal gravity, $\boldsymbol{\gamma}^n = \boldsymbol{\gamma}^w = \gamma\,\mathbf{n}$, in (3) or (4). The velocity indicated by the LN93 INS is then given (erroneously) by $\mathbf{v}_\gamma^w$, which satisfies the differential equation:

$$\frac{d}{dt}\mathbf{v}_\gamma^w = \mathbf{a}^w - \left(\boldsymbol{\omega}_{in}^w + \boldsymbol{\omega}_{ie}^w\right) \times \mathbf{v}_\gamma^w + \boldsymbol{\gamma}^w \tag{7}$$

That is, this is the equation that is integrated by the LN93 navigation computer to obtain the w-frame velocities. The latitude and longitude can be extracted directly from the transformation matrix, C_e^w, given by

$$C_e^w = \begin{pmatrix} -\cos\alpha\sin\phi\cos\lambda - \sin\alpha\sin\lambda & -\cos\alpha\sin\phi\sin\lambda + \sin\alpha\cos\lambda & \cos\alpha\cos\phi \\ \sin\alpha\sin\phi\cos\lambda - \cos\alpha\sin\lambda & \sin\alpha\sin\phi\sin\lambda + \cos\alpha\cos\lambda & -\sin\alpha\cos\phi \\ \cos\phi\cos\lambda & -\cos\phi\sin\lambda & -\sin\phi \end{pmatrix} \tag{8}$$

This matrix, an array of direction cosines, is also available with high precision in the LN93 output.

3.2 Two Approaches to Vector Gravimetry

There are now two approaches to estimating the gravity disturbance vector. The first approach uses an independent measurement of position (or velocity), such as from GPS, to compare against the INS-indicated position (or velocity). The difference is due to many sources of error, including the fact that only normal gravity, not the actual gravity vector, was used in the integration of (7).

The total error in indicated velocity satisfies a linear differential equation that is readily derived (using a linearity assumption for the error) from (4), as follows:

$$\frac{d}{dt}\delta\mathbf{v}^w = -\delta\left(\boldsymbol{\omega}_{iw}^w + \boldsymbol{\omega}_{ie}^w\right)\mathbf{v}^w - \left(\boldsymbol{\omega}_{iw}^w + \boldsymbol{\omega}_{ie}^w\right)\delta\mathbf{v}^w + \delta\mathbf{a}^w + \Gamma^w\,\delta\mathbf{p}^w + \delta\mathbf{g}^w \tag{9}$$

where $\Gamma^w\,\delta\mathbf{p}^w$ is the gravity gradient tensor multiplied by position errors in the w-frame (the horizontal components of the resulting vector are usually negligible). The acceleration error, $\delta\mathbf{a}^w$, further consists of sensor errors, $\delta\mathbf{a}^b$, and a Coriolis term due to orientation errors, $\boldsymbol{\psi}^w$, resulting from the erroneously computed transformation matrix, C_b^w:

$$\delta\mathbf{a}^w = C_b^w\,\delta\mathbf{a}^b + \mathbf{a}^w \times \boldsymbol{\psi}^w \tag{10}$$

These orientation errors satisfy their own differential equation given by (see Britting, 1971)

$$\dot{\boldsymbol{\psi}}^w = -\boldsymbol{\omega}_{iw}^w \times \boldsymbol{\psi}^w - C_b^w\,\delta\boldsymbol{\omega}_{ib}^b + \delta\boldsymbol{\omega}_{iw}^w \tag{11}$$

where $\delta\boldsymbol{\omega}_{ib}^b$ are the gyro errors. We note that $\delta\boldsymbol{\omega}_{iw}^w$ and $\delta\boldsymbol{\omega}_{ie}^w$ in (9) and (11) are also functions of errors in the velocity. Thus, together, (9) and (11) yield a system of linear differential equations for velocity and orientation errors. They describe a model for the dynamics of these errors.

The sensor errors and the gravity errors each have their own dynamics. The accelerometer error may comprise a bias (random constant), a scale factor error (random constant), correlated noise (e.g., a first-order Gauss-Markov process), and white noise. Similarly, the gyro error may consist of a drift (random constant), a scale factor error (random constant), correlated noise (first-order Gauss-Markov process), and white noise. Finally, the gravity error should be modeled as some kind of correlated process. Usually, a second- or third-order Gauss-Markov model is used. Including these dynamics into the basic dynamics system for the INS errors augments the system of linear differential equations significantly. The details of this are not given here; they may be found (for the case of n-frame coordinatization) in (Jekeli, 1995) and various other articles referenced therein.

The basic idea is to use a Kalman filter to distribute the position or velocity information, coming from an external source, such as GPS, in an optimal way so as to estimate the various errors of the system. One of these will be an estimate of the gravity error, that is the gravity disturbance vector. Again, the details of the formulations of the Kalman filter and all associated models are not pursued here. Only a schematic diagram is shown in Figure 6 to illustrate the essential processing technique. All details related to the processing of GPS phase data to obtain

positions (or velocities) are also omitted.

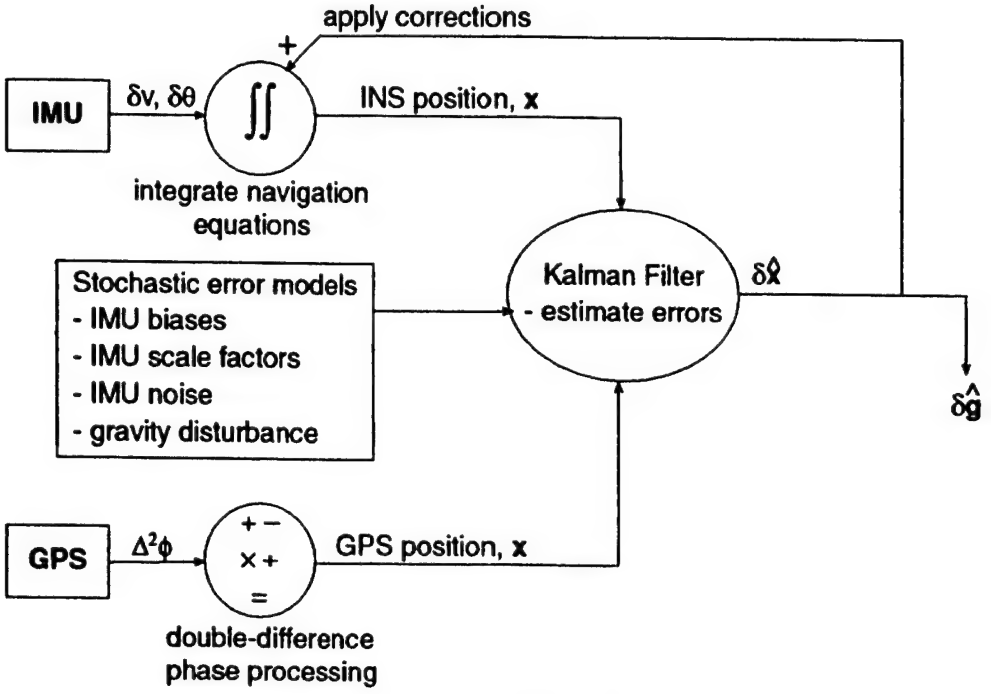

Figure 6: Traditional approach to estimate gravity disturbance from INS/GPS.

We note that the estimation of the gravity disturbance vector with this method absolutely requires that it be assigned a stochastic model. This can be a serious drawback to the method since the result may depend critically on the type of model chosen (see Jekeli, 1995). Furthermore, only the horizontal components of the gravity disturbance vector can be estimated this way since the integration of the inertial accelerations is quite unstable in the vertical (this is a well-known phenomenon that precludes free-inertial navigation in the vertical for periods longer than a few minutes).

The second approach is fundamentally different from the first. In this case no model for the gravity disturbance is required, at least in theory. Instead of time-integrating the IMU data to obtain positions (or velocities), the GPS positions are time-differentiated to obtain accelerations. These are then compared to the accelerations coming from the IMU's. One still has to account for Coriolis terms due to rotating frames, and the estimation of IMU errors can still be done with a Kalman filter, but the gravity disturbance is the result simply of a final differencing between two type of accelerations, fundamentally as alluded to by equation (1). This method is, in fact, precisely the way airborne scalar gravimetry is performed. Gravimeter measurements are corrected for the Eötvös effect and differenced with vertical accelerations determined from GPS, or a laser

altimeter, or the like.

In the case of the LN93, where raw acceleration data are not available, it is still possible to derive a method based on this principle. We simply take the indicated velocities and transform them back into accelerations with an appropriate numerical differentiation algorithm. From (1) and (2), we have

$$\delta \mathbf{g}^{w} = \mathbf{C}_{i}^{w}\, \ddot{\mathbf{x}}^{i} - \mathbf{a}^{w} - \boldsymbol{\gamma}^{w} \tag{12}$$

where $\mathbf{C}_{i}^{w}$ is the transformation matrix from the i-frame to the w-frame. Substituting (7) then yields

$$\delta \mathbf{g}^{w} = \mathbf{C}_{i}^{w}\, \ddot{\mathbf{x}}^{i} - \left[\frac{d}{dt}\mathbf{v}_{\gamma}^{w} + \left(\boldsymbol{\omega}_{iw}^{w} + \boldsymbol{\omega}_{ie}^{w}\right) \times \mathbf{v}_{\gamma}^{w}\right] \tag{13}$$

With $\mathbf{C}_{i}^{w} = \mathbf{C}_{e}^{w}\, \mathbf{C}_{i}^{e}$ and (5) we rewrite this as follows

$$\delta \mathbf{g}^{w} = \mathbf{C}_{e}^{w}\, \mathbf{C}_{i}^{e}\, \ddot{\mathbf{x}}^{i} - \left[\frac{d}{dt}\mathbf{v}_{\gamma}^{w} + \left(\boldsymbol{\omega}_{ew}^{w} + 2\, \mathbf{C}_{e}^{w}\, \boldsymbol{\omega}_{ie}^{e}\right) \times \mathbf{v}_{\gamma}^{w}\right] \tag{14}$$

where we note that $\mathbf{C}_{i}^{e}\, \ddot{\mathbf{x}}^{i} \neq \ddot{\mathbf{x}}^{e}$. Also, the transformation matrix, $\mathbf{C}_{i}^{e}$, and the angular rate, $\boldsymbol{\omega}_{ie}^{e}$, can be computed without error from Earth's rotation rate.

It is possible to determine, independently, the total acceleration $\mathbf{C}_{i}^{e}\, \ddot{\mathbf{x}}^{i}$ from GPS (the details, again, are omitted as being outside the scope of the present report). The transformation matrix, $\mathbf{C}_{e}^{w}$, is provided as output by the LN93 computer with high precision (although it also contains the same quantization error demonstrated in Figure 4, this will affect the acceleration computation at the part in 10^{7} level – about 0.1 mgal). The angular rate, $\boldsymbol{\omega}_{ew}^{w}$, is given by (6) (a more accurate form that accounts for ellipsoidal effects can be derived), and the w-frame velocities are provided by the LN93 with high precision. It remains, then, to differentiate these velocities numerically, and all quantities on the right and side of (14) are thus obtained. Therefore, it is possible to determine the gravity disturbance from indicated LN93 velocities and direction cosine matrix and from GPS accelerations. The errors arising form the IMU's must be treated in some way. This could be done in an optimal manner as discussed below for the case of raw data processing.

In the case that raw accelerometer and gyro data are available, as from CfM's LN100, one also has two data processing options available to estimate the gravity disturbance components. The traditional approach will not be described since it is identical to the case above, except that positions can now be determined independently of the navigation computer, thus ensuring

maximum computational precision (i.e., no artificial quantization effects). Only the second method based on a comparison of accelerations will be discussed in some detail. In particular, the processing of raw gyro and accelerometer data will be described in Section 3.3 following the essential formula for gravity disturbance computation.

This second approach to gravity disturbance vector estimation in the general sense has been considered by Jekeli and Garcia (1997), as well as by Schwarz and Li (1996). And, as already mentioned it is completely analogous to traditional scalar gravimetry, but extended to three dimensions. The essential idea is to combine equation (2) and equation (1) as follows:

$$\begin{aligned}\delta\mathbf{g}^n &= \mathbf{g}^n - \boldsymbol{\gamma}^n \\ &= \mathbf{C}_i^n\left(\ddot{\mathbf{x}}^i - \mathbf{C}_b^i\,\mathbf{a}^b\right) - \boldsymbol{\gamma}^n\end{aligned} \tag{15}$$

where $\mathbf{C}_b^i$ is the transformation to the i-frame from the body frame (b-frame), in which the inertial accelerations, $\mathbf{a}^b$, are measured. The transformation is obtained directly from the gyros of the INS, as shown below. This "direct differencing" method is much simpler computationally than the process indicated in Figure 6, and it uses data directly from the gyros and accelerometers, rather than integrating these data to the level of positions. On the other hand, the GPS position data must now be elevated to the level of acceleration. This means that noise in GPS position data is amplified at high frequencies and requires careful filtering.

3.3 Algorithms to Process Raw Gyro and Accelerometer Data

The IMU produces accelerometer and gyro pulses: $\delta\mathbf{v}_\ell$ and $\delta\boldsymbol{\theta}_\ell$, respectively; where $\delta\mathbf{v}_\ell$ is a vector of increments in the sensor-frame velocity generated by the three accelerometers, and $\delta\boldsymbol{\theta}_\ell$ is a vector of increments in the sensor-frame angles generated by the three gyros. With corresponding time increments, δt, we have

$$\delta\mathbf{v}_\ell = \int_{\delta t} \mathbf{a}^s(t)\,dt\ , \quad \delta\boldsymbol{\theta}_\ell = \int_{\delta t} \boldsymbol{\omega}_{is}^s(t)\,dt \tag{16a,b}$$

where $\mathbf{a}^s$ is the acceleration vector in the s-frame (sensor frame) and $\boldsymbol{\omega}_{is}^s$ is the angular rate with respect to the i-frame (inertial frame), also in the s-frame. Note that the integration takes place in the s-frame which is rotating with respect to the inertial frame. Also, we do not assume that the sensor and body frames are equivalent. In fact, in determining accelerations we must distinguish between the locations of the INS and the GPS antenna. This difference causes the so-called lever-arm effect. The body frame is usually associated with the aircraft and we will assume the GPS

antenna to be the origin of that frame. The s-frame has its origin located at some fiducial point on the INS, as specified by the manufacturer. The lever-arm effect is discussed later in Section 3.3.3.

To determine the acceleration in the i-frame, it is necessary to solve for the acceleration in the sensor frame using the δv_ℓ's, and then to rotate this into the i-frame using the orientation information contained in the $\delta\theta_\ell$'s. The rotation matrix, C_s^i, that transforms $\mathbf{a}^s$ into $\mathbf{a}^i$, according to $\mathbf{a}^s = C_s^i \mathbf{a}^s$ is determined by integrating a differential equation relating the angular rates to the rotation matrix:

$$\dot{C}_s^i = C_s^i \Omega_{is}^s \tag{17}$$

where Ω_{is}^s is a skew-symmetric matrix with components of ω_{is}^s as its off-diagonal elements:

$$\Omega_{is}^s = \begin{bmatrix} 0 & -\omega_3 & \omega_2 \\ \omega_3 & 0 & -\omega_1 \\ -\omega_2 & \omega_1 & 0 \end{bmatrix} \tag{18}$$

where $\omega_{is}^s = [\omega_1, \omega_2\, \omega_3]^T$.

It is far easier to formulate an equivalent differential equation in terms of quaternions. Let $\mathbf{q} = (a, b, c, d)^T$ be a four-vector of time-dependent quantities such that $\mathbf{q}$ satisfies the following linear system of differential equations

$$\dot{\mathbf{q}} = \frac{1}{2} A\, \mathbf{q} \tag{19}$$

where A is a 4x4 skew-symmetric matrix of time-dependent angular rates:

$$A = \begin{bmatrix} 0 & \omega_1 & \omega_2 & \omega_3 \\ -\omega_1 & 0 & \omega_3 & -\omega_2 \\ -\omega_2 & -\omega_3 & 0 & \omega_1 \\ -\omega_3 & \omega_2 & -\omega_1 & 0 \end{bmatrix} \tag{20}$$

It can be shown that

$$C_s^i = \begin{bmatrix} a^2 + b^2 - c^2 - d^2 & 2\,(bc + ad) & 2\,(bd - ac) \\ 2\,(bc - ad) & a^2 - b^2 + c^2 - d^2 & 2\,(cd + ab) \\ 2\,(bd + ac) & 2\,(cd - ab) & a^2 - b^2 - c^2 + d^2 \end{bmatrix} \tag{21}$$

The elements of $\mathbf{q}$ are known as *quaternions*. The integration of $\mathbf{q}$ is done incrementally over a time interval, such as δt, or a multiple of this; and, this gives the elements of C_s^i for each step.

3.3.1 A Second-Order Algorithm

Since the time increment for an IMU is usually very small; e.g., the data rate may be 256 Hz, so that $\delta t = 0.00390625$ s, it *may* be considered that $\boldsymbol{\omega}_{is}^s$ is constant over this time interval. It is not necessary to assume this; but then the integration formulas become more complicated, as seen in the subsequent section. For constant angular rates over δt, we have the estimate, from (16b), for the ℓ^{th} step:

$$\delta\hat{\boldsymbol{\theta}}_\ell = \boldsymbol{\omega}_{is}^s(t_\ell)\,\delta t \tag{22}$$

and, with matrix A assumed constant over this interval, denoted by $\hat{A}_\ell$, an analytic form of the solution to (19) can readily be found. It is

$$\hat{\mathbf{q}}(t) = e^{\frac{1}{2}\hat{A}_\ell (t - t_{\ell-1})}\,\hat{\mathbf{q}}(t_{\ell-1}) \;, \quad 0 \le t - t_{\ell-1} \le \delta t \tag{23}$$

which, in series form, yields the following iterative solution:

$$\hat{\mathbf{q}}(t_\ell) = \left(I + \tfrac{1}{2}\hat{A}_\ell\,\delta t + \tfrac{1}{8}\hat{A}_\ell^2\,\delta t^2 + \tfrac{1}{48}\hat{A}_\ell^3\,\delta t^3 + \ldots\right)\hat{\mathbf{q}}(t_{\ell-1}) \;, \quad \ell = 1,2,\ldots \tag{24}$$

where a single initial condition, $\hat{\mathbf{q}}(t_0)$, must be specified. A corresponding closed form may be found by noting that the powers of the matrix $\hat{A}_\ell$ are either diagonal (even powers) or proportional to $\hat{A}_\ell$ itself (odd powers). One has:

$$\hat{\mathbf{q}}(t_\ell) = \left[\cos\left(\tfrac{1}{2}\left|\delta\hat{\boldsymbol{\theta}}_\ell\right|\right) I + \frac{1}{\left|\delta\hat{\boldsymbol{\theta}}_\ell\right|}\sin\left(\tfrac{1}{2}\left|\delta\hat{\boldsymbol{\theta}}_\ell\right|\right)\hat{B}_\ell\right]\hat{\mathbf{q}}(t_{\ell-1}) \tag{25}$$

where $\left|\delta\hat{\boldsymbol{\theta}}_\ell\right| = \sqrt{\delta\hat{\boldsymbol{\theta}}_\ell^T\delta\hat{\boldsymbol{\theta}}_\ell}$ and

$$\hat{B}_\ell = \hat{A}_\ell\,\delta t \tag{26}$$

The solution (24) is given, in principle, with two errors, an algorithm error (the solution (23) assumed constant A-matrix) and a data error, both due to the assumption of constant angular rates.

However, the data error, in a sense, is fictitious since the data are not the angular rates, as approximated by $\hat{A}_\ell$, but the integrals given by (16b). Thus, let

$$B_\ell = \int_{t_{\ell-1}}^{t_\ell} A(t)\, dt \tag{27}$$

Using B_ℓ instead of $\hat{A}_\ell \delta t$ in (24) yields the actual algorithm

$$\hat{q}(t_\ell) = \left(I + \frac{1}{2} B_\ell + \frac{1}{8} B_\ell^2 + \frac{1}{48} B_\ell^3 + ...\right) \hat{q}(t_{\ell-1}), \quad \ell = 1,2,... \tag{28}$$

This formula, however, still contains algorithm error.

This algorithm error is of the order δt^3. Indeed, let the true quaternion be represented over the integration interval by the series

$$q(t_\ell) = q(t_{\ell-1}) + \dot{q}(t_{\ell-1})\, \delta t + \frac{1}{2!} \ddot{q}(t_{\ell-1})\, \delta t^2 + \frac{1}{3!} \dddot{q}(t_{\ell-1})\, \delta t^3 + ... \tag{29}$$

Substituting (19) yields

$$\begin{aligned} q_\ell = \Big[I + \tfrac{1}{2} A_{\ell-1}\, \delta t + \tfrac{1}{4}\Big(\dot{A}_{\ell-1} + \tfrac{1}{2} A_{\ell-1}^2\Big)\, \delta t^2 \\ + \tfrac{1}{12}\Big(\ddot{A}_{\ell-1} + \dot{A}_{\ell-1} A_{\ell-1} + \tfrac{1}{2} A_{\ell-1} \dot{A}_{\ell-1} + \tfrac{1}{4} A_{\ell-1}^3\Big)\, \delta t^3 + ...\Big]\, q_{\ell-1} \end{aligned} \tag{30}$$

where all quantities are true, not approximate, and subscripts denote the time epoch at which they are defined. Similarly, from (27) we may write in terms of true quantities:

$$B_\ell = A_{\ell-1}\, \delta t + \frac{1}{2} \dot{A}_{\ell-1}\, \delta t^2 + \frac{1}{6} \ddot{A}_{\ell-1}\, \delta t^3 + ... \tag{31}$$

Substituting (31) into (28) and comparing with (30), it is easily verified that the algorithm error is

$$\hat{q}_\ell - q_\ell = \Big[\tfrac{1}{48}\Big(A_{\ell-1} \dot{A}_{\ell-1} - \dot{A}_{\ell-1} A_{\ell-1}\Big)\, \delta t^3 + ...\Big]\, q_{\ell-1} \tag{32}$$

assuming the previous error, $\hat{q}_{\ell-1} - q_{\ell-1}$, yields higher-order terms.

It can be shown that the first term in (32) vanishes if the angular rate vector does not change direction during the integration interval; i.e., in that case the A-matrix and its first derivative commute. That is why the algorithm (28) is said to have *commutativity error*, or *coning error*. In other words, if the angular rate vector *does* change direction, the system is "coning".

3.3.2 A Third-Order Algorithm

One can design higher-order algorithms in a number of ways. One is to do a numerical integration of (19) based on a model for the angular rates. The Runge-Kutta (R.K.) algorithm is one such integrator; and, in turns out that the third order R.K. method with a linear model for the angular rates yields an algorithm for the quaternions with fourth-order algorithm error. The third-order R.K. method requires that the function being integrated is evaluated at either end of the integration interval and half-way in between. Therefore, in this case the integration interval is twice the data interval:

$$\Delta t = 2\,\delta t \tag{33}$$

To simplify the notation, let $\boldsymbol{\omega}_{is}^{s}(t) \equiv \boldsymbol{\omega}(t)$, and assume that over the integration interval:

$$\boldsymbol{\omega}(t) = \boldsymbol{\omega}_{\ell-2} + \dot{\boldsymbol{\omega}}_{\ell-2}\,(t - t_{\ell-2}) + O(\Delta t^2) \;; \quad |t - t_{\ell-2}| \le \Delta t \tag{34}$$

where the subscripts denote evaluation of the (true) quantity at the corresponding epochs spanning intervals δt , *not* Δt . Substituting (34) into (16b) yields

$$\delta\boldsymbol{\theta}_{\ell-1} = \int_{t_{\ell-2}}^{t_{\ell-1}} \boldsymbol{\omega}(t')\,dt' = \boldsymbol{\omega}_{\ell-2}\,\delta t + \frac{1}{2}\,\dot{\boldsymbol{\omega}}_{\ell-2}\,\delta t^2 + O(\Delta t^3) \tag{35}$$

$$\delta\boldsymbol{\theta}_{\ell} = \int_{t_{\ell-1}}^{t_{\ell}} \boldsymbol{\omega}(t')\,dt' = \boldsymbol{\omega}_{\ell-2}\,\delta t + \frac{3}{2}\,\dot{\boldsymbol{\omega}}_{\ell-2}\,\delta t^2 + O(\Delta t^3) \tag{36}$$

Solving for $\boldsymbol{\omega}_{\ell-2}$ and $\dot{\boldsymbol{\omega}}_{\ell-2}$, it is readily verified that

$$\boldsymbol{\omega}_{\ell-2} = \frac{1}{2\delta t}(3\,\delta\boldsymbol{\theta}_{\ell-1} - \delta\boldsymbol{\theta}_{\ell}) + O(\Delta t^2) \tag{37}$$

$$\dot{\omega}_{\ell-2} = \frac{1}{\delta t^2}\left(\delta\theta_\ell - \delta\theta_{\ell-1}\right) + O(\Delta t) \tag{38}$$

Using these expressions in (34) yields for three consecutive epochs:

$$\omega_{\ell-2}\,\Delta t = 3\,\delta\theta_{\ell-1} - \delta\theta_\ell + O(\Delta t^3) \tag{39}$$

$$\omega_{\ell-1}\,\Delta t = \delta\theta_{\ell-1} + \delta\theta_\ell + O(\Delta t^3) \tag{40}$$

$$\omega_\ell\,\Delta t = 3\,\delta\theta_\ell - \delta\theta_{\ell-1} + O(\Delta t^3) \tag{41}$$

Therefore, we have the following observed quantities, which are accurate in terms of the model to second order:

$$\hat{\omega}_{\ell-2}\,\Delta t = 3\,\delta\theta_{\ell-1} - \delta\theta_\ell \tag{42}$$

$$\hat{\omega}_{\ell-1}\,\Delta t = \delta\theta_{\ell-1} + \delta\theta_\ell \tag{43}$$

$$\hat{\omega}_\ell\,\Delta t = 3\,\delta\theta_\ell - \delta\theta_{\ell-1} \tag{44}$$

With the Taylor expansions (35) and (36) substituted into the right sides, we also obtain

$$\hat{\omega}_{\ell-2}\,\Delta t = \omega_{\ell-2}\,\Delta t + O(\Delta t^3) \tag{45}$$

$$\hat{\omega}_{\ell-1}\,\Delta t = \omega_{\ell-2}\,\Delta t + \frac{1}{2}\,\dot{\omega}_{\ell-2}\,\Delta t^2 + O(\Delta t^3) \tag{46}$$

$$\hat{\omega}_\ell\,\Delta t = \omega_{\ell-2}\,\Delta t + \dot{\omega}_{\ell-2}\,\Delta t^2 + O(\Delta t^3) \tag{47}$$

The third-order R.K. algorithm, for $\dot{\mathbf{q}} = \mathbf{f}(\mathbf{q},t)$, is given by

$$\hat{\mathbf{q}}_\ell = \hat{\mathbf{q}}_{\ell-2} + \frac{1}{6}\left(\Delta\mathbf{q}_0 + 4\,\Delta\mathbf{q}_1 + \Delta\mathbf{q}_2\right) \tag{48}$$

where

$$\Delta \mathbf{q}_0 = \mathrm{f}\left(\hat{\mathbf{q}}_{\ell-2},\, t_{\ell-2}\right) \Delta t \tag{49}$$

$$\Delta \mathbf{q}_1 = \mathrm{f}\left(\hat{\mathbf{q}}_{\ell-2} + \frac{1}{2}\Delta \mathbf{q}_0,\, t_{\ell-1}\right) \Delta t \tag{50}$$

$$\Delta \mathbf{q}_2 = \mathrm{f}\left(\hat{\mathbf{q}}_{\ell-2} + 2\,\Delta \mathbf{q}_1 - \Delta \mathbf{q}_0,\, t_{\ell}\right) \Delta t \tag{51}$$

This iterative integration algorithm provides an approximate solution at intervals of Δt; but one could do a second iteration, using the same data, on the in-between points - it is just a matter of which starting value is chosen. Note that only one starting quaternion is required; the R.K. algorithm is a single-step method.

From (19), we have $\mathrm{f}(\mathbf{q}, t) = \mathrm{A}(t)\,\mathbf{q}/2$; and using the observed values (42) - (44) for $\mathrm{A}(t_{\ell-2})$, $\mathrm{A}(t_{\ell-1})$, $\mathrm{A}(t_{\ell})$, equations (49) - (51) become with $\hat{\mathrm{B}}_{\ell} = \hat{\mathrm{A}}_{\ell}\,\Delta t$ (from (42) - (44)):

$$\Delta \mathbf{q}_0 = \frac{1}{2}\,\hat{\mathrm{B}}_{\ell-2}\,\hat{\mathbf{q}}_{\ell-2} \tag{52}$$

$$\Delta \mathbf{q}_1 = \frac{1}{2}\,\hat{\mathrm{B}}_{\ell-1}\left(\mathrm{I} + \frac{1}{4}\,\hat{\mathrm{B}}_{\ell-2}\right)\hat{\mathbf{q}}_{\ell-2} \tag{53}$$

$$\Delta \mathbf{q}_2 = \frac{1}{2}\,\hat{\mathrm{B}}_{\ell}\left[\mathrm{I} + \hat{\mathrm{B}}_{\ell-1}\left(\mathrm{I} + \frac{1}{4}\,\hat{\mathrm{B}}_{\ell-2}\right) - \frac{1}{2}\,\hat{\mathrm{B}}_{\ell-2}\right]\hat{\mathbf{q}}_{\ell-2} \tag{54}$$

Substituting these into (48) and simplifying the result yields

$$\hat{\mathbf{q}}_{\ell} = \left[\mathrm{I} + \frac{1}{12}\left(\hat{\mathrm{B}}_{\ell} + 4\,\hat{\mathrm{B}}_{\ell-1} + \hat{\mathrm{B}}_{\ell-2}\right) + \frac{1}{12}\left(\mathrm{I} + \frac{1}{4}\,\hat{\mathrm{B}}_{\ell}\right)\hat{\mathrm{B}}_{\ell-1}\,\hat{\mathrm{B}}_{\ell-2} + \frac{1}{12}\,\hat{\mathrm{B}}_{\ell}\left(\hat{\mathrm{B}}_{\ell-1} - \frac{1}{2}\,\hat{\mathrm{B}}_{\ell-2}\right)\right]\hat{\mathbf{q}}_{\ell-2} \tag{55}$$

By substituting (45) - (47) into (55), it is readily verified, with a comparison to (30), that

$$\hat{\mathbf{q}}_{\ell} - \mathbf{q}_{\ell} = \mathrm{O}\left(\delta t^4\right)\mathbf{q}_{\ell-1} \tag{56}$$

That is, equation (55) is a third-order algorithm; the algorithm error is of fourth order.

Higher order algorithms can be derived, but they will require larger integration intervals per step (if the basic data interval, δt, remains the same).

The initial value for the iteration, $\mathbf{q}_0$ (or, $\mathbf{q}_1$), is obtained from the initialization (alignment) of

the IMU, typically provided by the navigation computer. Or one can determine the initial attitude externally using (zero) velocity updates in a Kalman filter using standard procedures. If the result is an initial rotation matrix the following inverse relationship to (21) can be used to get the initial quaternion:

$$
\begin{aligned}
a &= \frac{1}{2}\left(1 + (C_s^i)_{1,1} + (C_s^i)_{2,2} + (C_s^i)_{3,3}\right)^{1/2} \\
b &= \frac{1}{4a}\left((C_s^i)_{2,3} - (C_s^i)_{3,2}\right) \\
c &= \frac{1}{4a}\left((C_s^i)_{3,1} - (C_s^i)_{1,3}\right) \\
d &= \frac{1}{4a}\left((C_s^i)_{1,2} - (C_s^i)_{2,1}\right)
\end{aligned}
\tag{57}
$$

These equations are readily verified since C_s^i is an orthogonal matrix, where

$$C_s^i = C_n^i\, C_s^n \tag{58}$$

and n denotes the navigation frame (n-frame). C_s^n is obtained during the initialization phase and C_n^i can be determined from the known position of the system at the initial time.

Finally, it is noted that the quaternions must satisfy the following property:

$$a^2 + b^2 + c^2 + d^2 = 1 \tag{59}$$

On the other hand, the computed quaternions, $\hat{\mathbf{q}}$, from any algorithm may not satisfy this constraint. This is due to numerical round-off error as well as model error and will cause the computed transformation matrix to become non-orthogonal. To avoid this it is advisable (practically necessary) to "re-orthogonalize" the computed quaternions at each iteration according to

$$\hat{\mathbf{q}} \leftarrow \frac{1}{\sqrt{\hat{\mathbf{q}}^T \hat{\mathbf{q}}}}\,\hat{\mathbf{q}} \tag{60}$$

which will ensure that $\hat{\mathbf{q}}^T \hat{\mathbf{q}} = 1$ and that $\hat{C}_b^a$ is orthogonal.

3.3.3 Lever-Arm Effect

Consider the sensor frame to be attached to the IMU, as before. In order to compare the inertial accelerations determined at the IMU with the inertial accelerations determined by GPS at the GPS antenna, it is necessary to correct for the lever-arm effects of the IMU with respect to the antenna (or vice versa). Without loss in generality, one may assume that the b-frame and s-frame are parallel; but their origins are offset by the lever arm, $\mathbf{b}^b$, the vector of coordinates of the sensor (IMU) in the b-frame (Figure 7).

We have the following relationship

$$\mathbf{b}^i = \mathbf{x}^i_{accel} - \mathbf{x}^i_{body} \tag{61}$$

where all coordinates are in the i-frame. The acceleration of the b-frame can be expressed in terms of the sensed accelerations in the s-frame by applying the the Coriolis law to (61), noting that $\dot{\mathbf{b}}^b = \mathbf{0}$ (the two frames are rigidly connected, by assumption):

$$\dot{\mathbf{x}}^i_{accel} = \dot{\mathbf{x}}^i_{body} + \dot{\mathbf{b}}^i = \dot{\mathbf{x}}^i_{body} + \mathbf{C}^i_b\, \boldsymbol{\omega}^b_{ib} \times \mathbf{b}^b \tag{62}$$

Differentiating again, we obtain

$$\ddot{\mathbf{x}}^i_{accel} = \ddot{\mathbf{x}}^i_{body} + \left(\dot{\mathbf{C}}^i_b\, \boldsymbol{\omega}^b_{ib} + \mathbf{C}^i_b\, \dot{\boldsymbol{\omega}}^b_{ib}\right) \times \mathbf{b}^b = \ddot{\mathbf{x}}^i_{body} + \mathbf{C}^i_b\, \dot{\boldsymbol{\omega}}^b_{ib} \times \mathbf{b}^b + \mathbf{C}^i_b\, \boldsymbol{\omega}^b_{ib} \times \left(\boldsymbol{\omega}^b_{ib} \times \mathbf{b}^b\right) \tag{63}$$

Coordinatizing this in the b-frame using $\mathbf{C}^b_i$, we have with $\ddot{\mathbf{x}}^i = \mathbf{a}^i + \mathbf{g}^i$ from (1):

$$\mathbf{C}^b_s\, \mathbf{a}^s_{accel} = \mathbf{a}^b_{accel} = \mathbf{a}^b_{body} + \mathbf{g}^b_{body} - \mathbf{g}^b_{accel} + \dot{\boldsymbol{\omega}}^b_{ib} \times \mathbf{b}^b + \boldsymbol{\omega}^b_{ib} \times \left(\boldsymbol{\omega}^b_{ib} \times \mathbf{b}^b\right) \tag{64}$$

where it is assumed that $\mathbf{C}^s_b = \mathbf{I}$. This says that the acceleration sensed in the s-frame, but coordinatized in the b-frame to which it is rigidly attached, is equal to the acceleration of the b-frame plus various reaction forces supplied by the rigid support of the s-frame to the b-frame. The first is due to the gravitational difference between locations of the accelerometer and case frame origins, and the others are associated with the rotation of the case in the i-frame. $\mathbf{g}^b$ is the gravitation vector at the indicated point in the b-frame; the only component of concern is the vertical component which varies by about -0.3086 mgal/m.

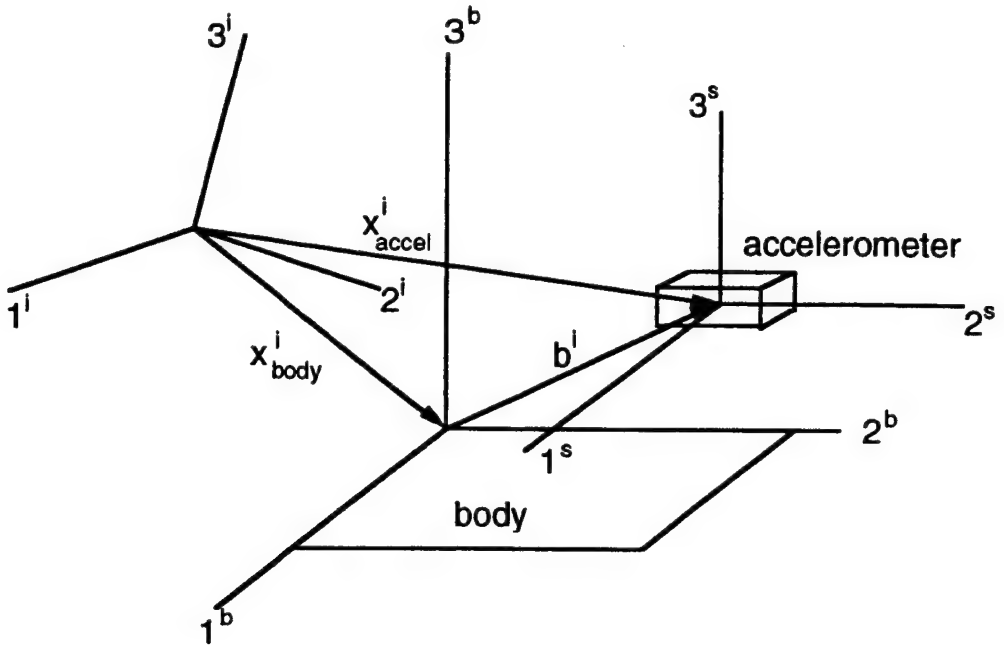

Figure 7. Accelerometer (sensor) and body frames relative to the i-frame.

Alternative formulas for the lever-arm effect from a practical viewpoint can be derived for the case of twice differentiating lever-arm positions in the i-frame:

$$\mathbf{a}^b_{accel} = \mathbf{a}^b_{body} + \mathbf{g}^b_{body} - \mathbf{g}^b_{accel} + C^b_i \frac{d^2}{dt^2}\left(C^i_b \mathbf{b}^b\right) \tag{65}$$

and for the case of once differentiating lever-arm velocities, also in the i-frame:

$$\mathbf{a}^b_{accel} = \mathbf{a}^b_{body} + \mathbf{g}^b_{body} - \mathbf{g}^b_{accel} + C^b_i \frac{d}{dt}\left(C^i_b \omega^b_{ib} \times \mathbf{b}^b\right) \tag{66}$$

It is readily verified that (65) and (66) are equivalent to (64). For the practical computations, in both cases, it is necessary to know the transformation, C^i_b, from the body frame to the inertial frame. For the latter case, also the angular rate of rotation, ω^b_{ib}, must be known. These quantities are determined from the gyro data using an algorithm such as described in Section 3.3.2. Note that the transformation of the lever-arm to the i-frame must be done before implementing a time-differentiation algorithm. Experiments have shown that these formulas are more stable and accurate than (64) since the latter requires a numerical time-differentiation of the angular rate, ω^b_{ib}.

3.3.4 Final Computation

To compute the sensed accelerations form the accelerometer output data (16a), we may use a first-order estimate:

$$\hat{\mathbf{a}}_\ell^s = \frac{1}{2\delta t}(\delta \mathbf{v}_{\ell+1} + \delta \mathbf{v}_\ell) \tag{67}$$

Having determined the quaternions, $\mathbf{q}(t_\ell)$, using (55), one computes $C_s^i(t_\ell)$ from (21). At the same time, the lever-arm effects are applied to the measured accelerations (67) according to (65), or (66). The normal gradient of gravitation should be used if there is a significant vertical component in the lever-arm. The result is the b-frame accelerations, $\mathbf{a}^b(t_\ell)$, at the GPS antenna. Then, since $C_b^i(t_\ell) = C_s^i(t_\ell)$, there is

$$\mathbf{a}^i(t_\ell) = C_b^i(t_\ell)\, \mathbf{a}^b(t_\ell) \tag{68}$$

where $\mathbf{a}^i(t_\ell)$ is the inertial acceleration in the i-frame. This can be compared directly to the GPS-derived kinematic acceleration in the i-frame, $\ddot{\mathbf{x}}^i$, to get the gravitation vector in the i-frame:

$$\mathbf{g}^i = \ddot{\mathbf{x}}^i - \mathbf{a}^i \tag{69}$$

It remains only to transform the gravitation vector into more appropriate coordinates, the n-frame:

$$\mathbf{g}^n = C_i^n\, \mathbf{g}^i \tag{70}$$

where, again, C_n^i can be determined from the position of the GPS antenna. The accuracy of C_n^i need be only 1 part in 10^6 to get mgal accuracy in the gravitation vector.

This scheme so far does not account for the IMU errors. One method to estimate these errors is to use a Kalman filter on a model for the accelerations, where the GPS-derived accelerations serve as updates to the filter. The residual between the observed GPS accelerations and the "adjusted" GPS accelerations would indicate the gravity disturbance. In this case no stochastic model for the gravity disturbance is required as in the case of Kalman-filtering INS positions. A schematic of this procedure is given in Figure 8.

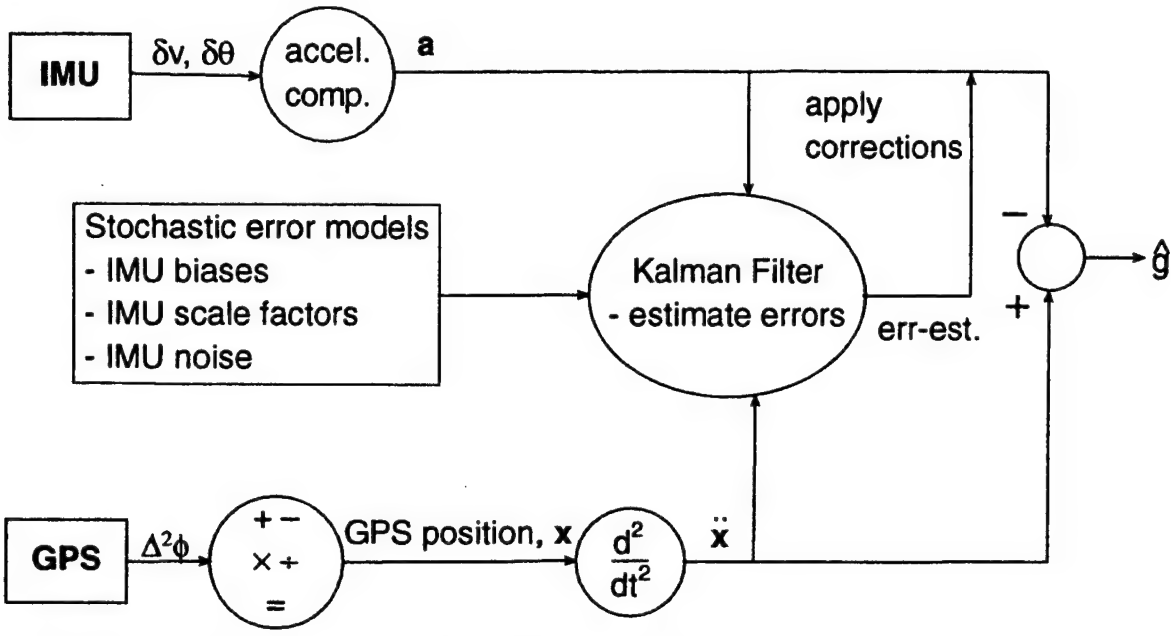

Figure 8: Alternative Data Processing for Vector Gravimetry

4 Tests and Analysis with the LN93 and LN100

Much of the difficulties surrounding the use of the LN93 centered on understanding the user interface software supplied with the system. The software, written in Pascal, is authored by Litton and is called the User-Friendly Bus Control (UFBC) software. It is written for the desk-top personal computer and a Pentium based system is recommended. Furthermore, since a high volume of data from the INS must be written to data storage very quickly, a RAMDRIVE must be set up in RAM; at least 10 MB of memory must be available for the RAMDRIVE. Some details on the individual components of the interface are documented in the report by Humphrey and Kawakami (1996).

Figure 9 shows a schematic of the system interrupts that are used to control the timing and data requests of the 1553 bus controller. The timing of the INS data is crucial since the difference between GPS and INS clocks can amount to significant lags. The entire data retrieval from the INS is governed by GPS time. A signal, called the PPS (pulse-per-second), is sent by the GPS receiver through the timer card to the PC. The PPS is synchronized to GPS time to within a millisecond, or better, depending on the receiver. Receipt of the PPS by the PC initiates a sequence of events. First, a "no-data" message is sent to the INS, causing a bit-failure in the system indicating a timer problem. This causes the INS clock to be reset to zero. This clock is a

counter that fills a 16-bit register with 64 microsecond counts. After about 4.2 s, the counter "turns over" to zero; thus a reset from the GPS PPS will yield an unambiguous time tag from the INS between zero and one second for each retrieved data item. It is only necessary to identify the PPS in terms of absolute time from the GPS receiver.

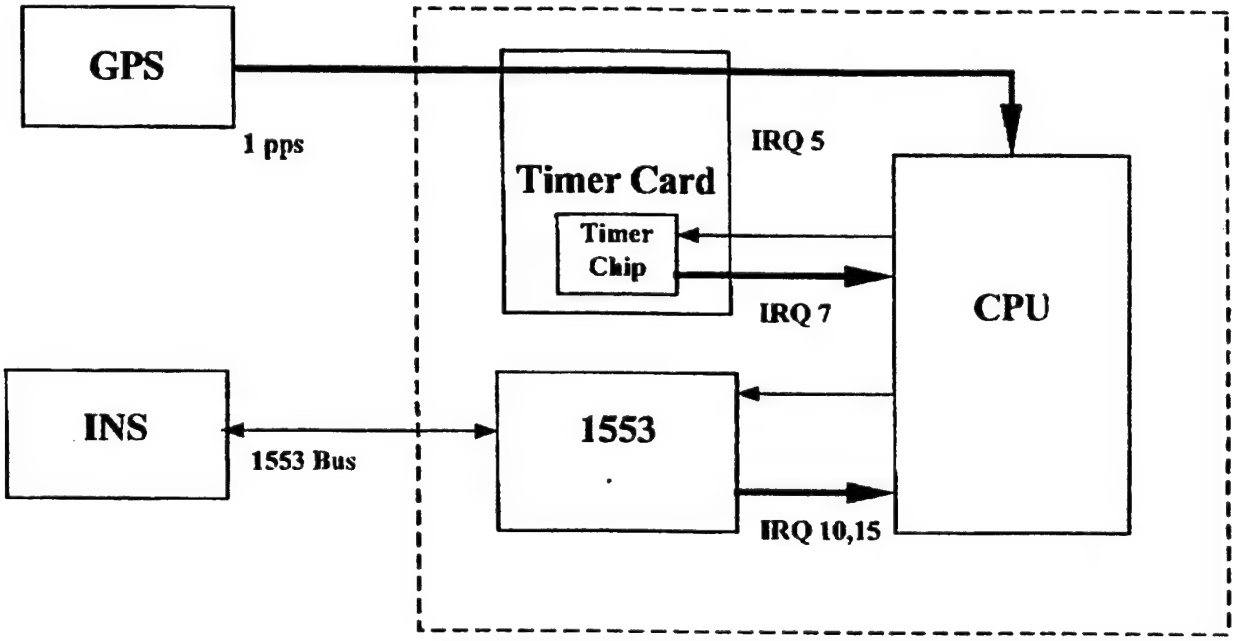

Figure 9: Interrupts that control the timing of INS data requests.

The next event triggered by the receipt of the PPS is the start of a clock on the timer board that counts off 0.05 seconds, where each count serves to identify the next request of data from the INS through the 1553 bus. It is noted that the time tags of the INS data refer to the time of validity of the data computed by the INS, for example, the velocity or position coordinates. These time epochs reflect the time at which the raw data were sampled to compute the position or velocity. Since there is a significant time (typically < 0.1 s) associated with these computations, the time tag at the epoch of the PPS, and for two epochs beyond this, actually refers to the previous PPS. This is important to note for the proper interpretation of the time tags of the INS data relative to the GPS time.

It is also noted that the bit-failure caused by the no-data message prevents the INS from optimally initializing the INS and entering into the NAV-READY mode. To circumvent the bit-failure on initialization, a different bus controller file (that does not send this message) is used to allow the INS to achieve the NAV-READY mode. Once NAV-READY is achieved, a new bus controller file must be initiated by the user.

The UFBC software was modified to allow the option of running the INS without GPS time synchronization. This proved useful in tests of the UFBC software and in laboratory tests where only the navigation error characteristics of the LN93 were to be investigated.

Some difficulties that plagued the LN93 system integration included the failure to adapt the UFBC software to retrieve and save also the GPS data from the receiver. This may be due to the high I/O rates that are imposed on the system, causing failures in saving any of the required data. It was judged that the GPS receiver should save the GPS data independently of the INS, where, of course, the same PPS time tags are applied to the GPS data. Other problems that needed to be overcome for practical system integration concerned providing appropriate power from 12-VDC batteries, or from 28-VDC aircraft power, to the 28 VDC input power of the INS, the 120VAC input power of the PC, and the 12VDC input power of the GPS receiver.

Initial tests of the LN93 were done in the laboratory in order to understand the INS output data and check out the general operation of the system. These test were followed by road tests, where the INS was strapped in the back of a van and driven over a period of about 45 minutes in the area of Columbus. Figure 10 shows the closed course followed for three such tests. One course could not be completed due to a power failure just prior to returning to the start point. The misclosure, calculated as the total distance between the true and indicated end points for each course, on average, was 670 m. This is well within the 0.8 nmi/hr = 1.4 km/hr specified for the system; and it shows that the LN93 is performing as expected, or better.

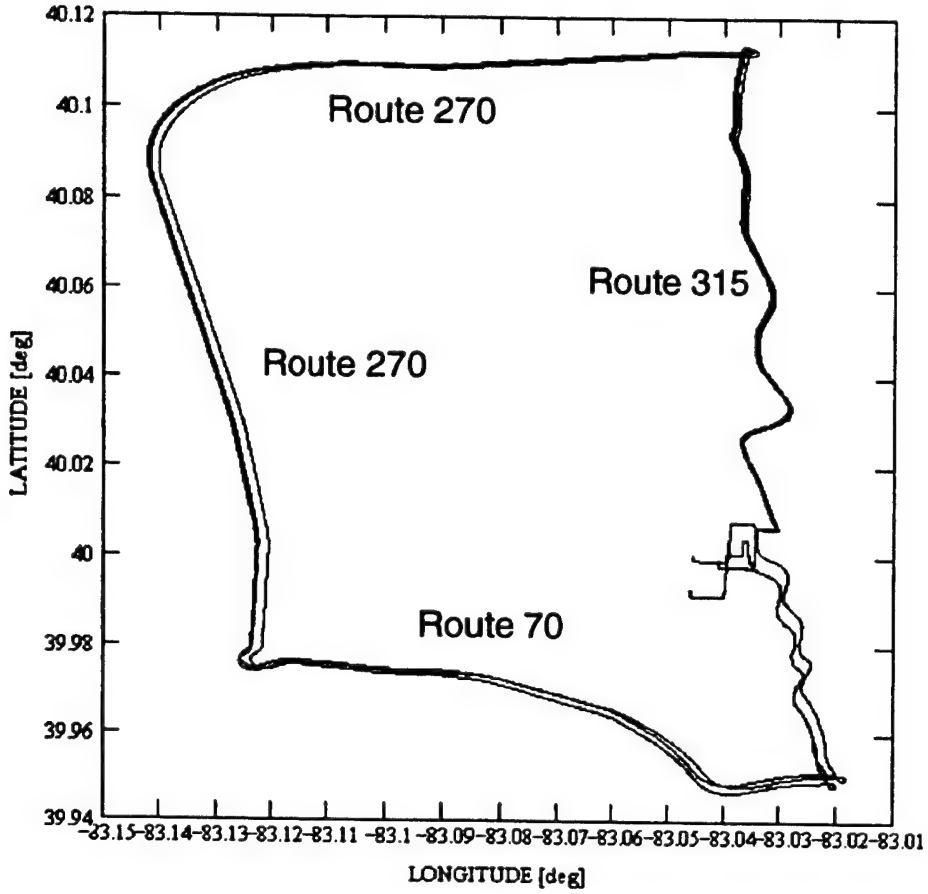

Figure 10: Van Tests of LN93 in Columbus Area

During these road tests, GPS data were also collected using a Trimble 4100 SSI receiver, but the results were rather poor due to frequent signal outages caused by many overpasses and other obstructions. It was not deemed worthwhile to attempt further tests with the integrated GPS/INS on the van at this time because of the difficulties of GPS data collection, the frequent power problems that were encountered, and the difficulties of adapting the UFBC software to the specific applications at hand.

Finally, some effort was undertaken to conduct an airborne test of the LN93. In collaboration with the Ohio Department of Transportation (ODOT), a cradle was constructed for the INS that could be slipped onto the seat rails of a small twin-engine photogrammetric aircraft. One test was conducted but ended in failure because of a power interruption to the system during landing and UFBC data handling problems. Future tests may be resumed on an opportunity basis.

The Center for Mapping (CfM) at OSU has developed an Airborne Integrated Mapping System (AIMS) that includes a Trimble GPS receiver and a Litton LN100 INS (Grejner-Brzezinska and

Phuyal, 1998). This system has undergone numerous flight tests and the data from one of the early tests were analyzed to determine the viability of this system for vector gravimetry. Ground tests conducted by CfM similar to those described above indicated that also the LN100 was performing at the specified level of 0.6 nmi/hr = 1 km/hr.

The test flight that was analyzed was conducted in the St. Louis, Missouri, area; and the indicated (i.e., free-inertial) INS and GPS trajectories are shown in Figure 11. The misclosure of the INS trajectory is about 30 km after less than one hour of flight, probably due to excessive errors in the gyro data (clearly, the system did not perform within specification during this test). Grejner-Brzezinska and Phuyal (1998) report that for this test flight the attitude error estimated using a Kalman and GPS position updates had standard deviations up to 17 arcsec (rms). Therefore, this flight test was not particularly suitable for the purpose of vector gravimetry.

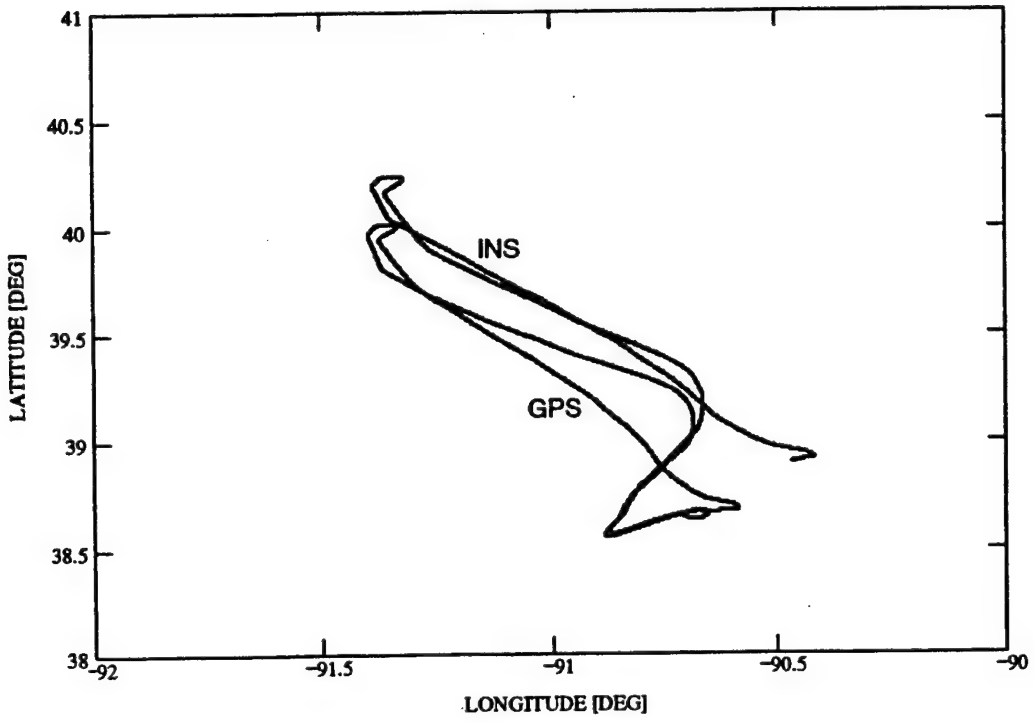

Figure 11: INS and GPS trajectories of Flight #3, CfM, 3/6/97.

However, in order to test the Kalman filter software for estimating the gravity disturbance vector, and because the trajectory included a relatively straight path, the data were analyzed. The actual deflection of the vertical along the flight path was interpolated from a 2'x2' DOV data base provided by the National Imaging and Mapping Agency (NIMA). Figure 12 shows the relative

deflections along the flight path; and Figure 13 shows the estimated deflections, the actual deflections, and their differences. The Kalman filter that was used to estimate the deflections included the error states noted in Table 2, as well as a correlated noise model (first-order Gauss-Markov) for the accelerometers with variance equal to 25 $mgal^2$ and a correlation time of 5 min. The gravity disturbance model was a third-order Gauss Markov model with variance equal to 480 $mgal^2$ and a correlation distance of about 26 km.

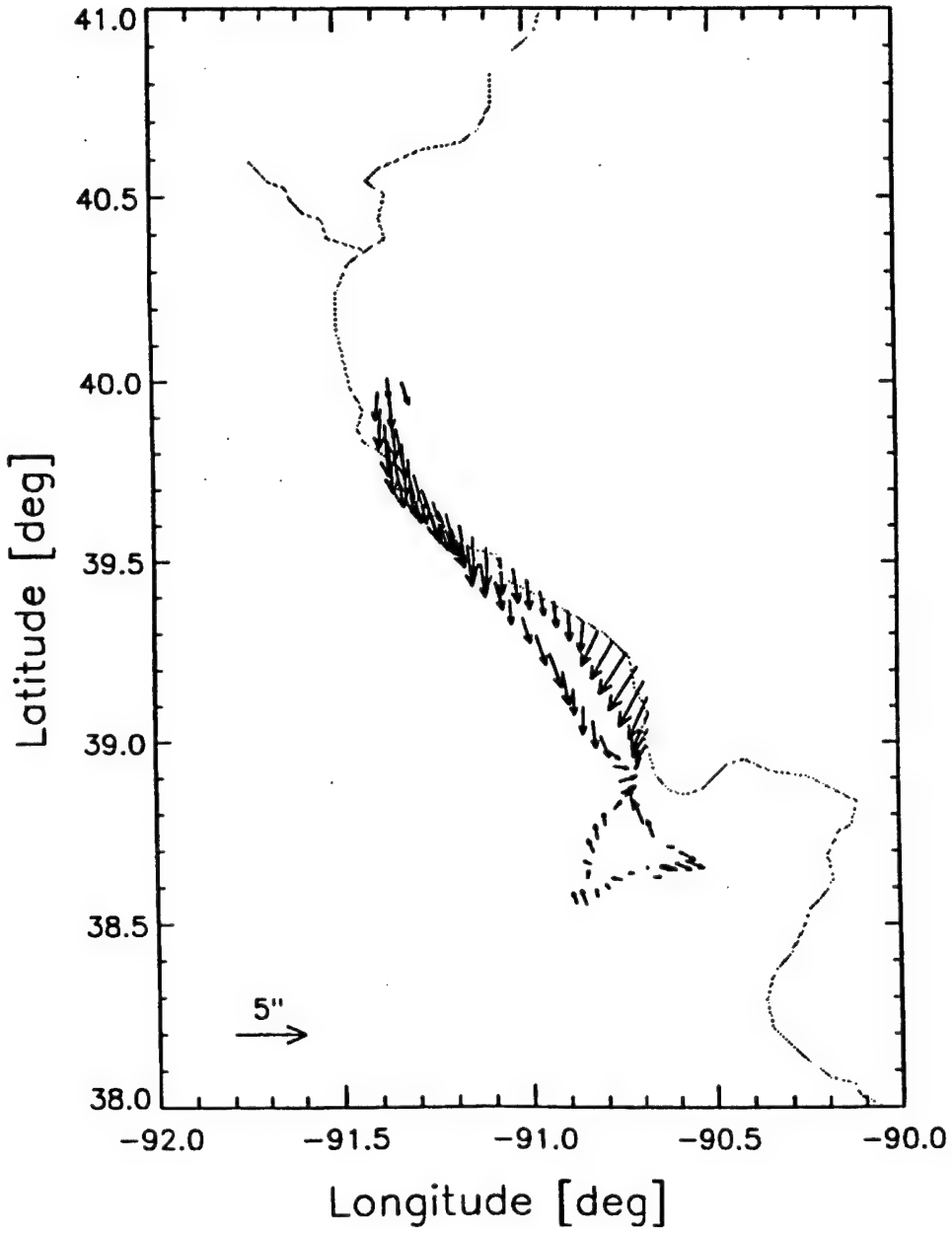

Figure 12. Vertical deflection differences with respect to initial point.

The results of the estimations are rather poor as seen in Figure 13. The errors in the estimated deflections are as large as the deflections themselves. This is very likely due to the large errors in the gyros. However, the east deflection error consists primarily of a trend and may reflect the fact that the north gyro (whose errors contribute to the east deflection error) is always easier to calibrate during INS initialization than the east gyro. We also see from Figure 11 that most of the position error (at least initially) is in the north direction, again pointing to large east gyro errors. Thus, while the numerical results of this test are not satisfactory, there is some indication that we understand the reason for this, which in itself is a useful conclusion.

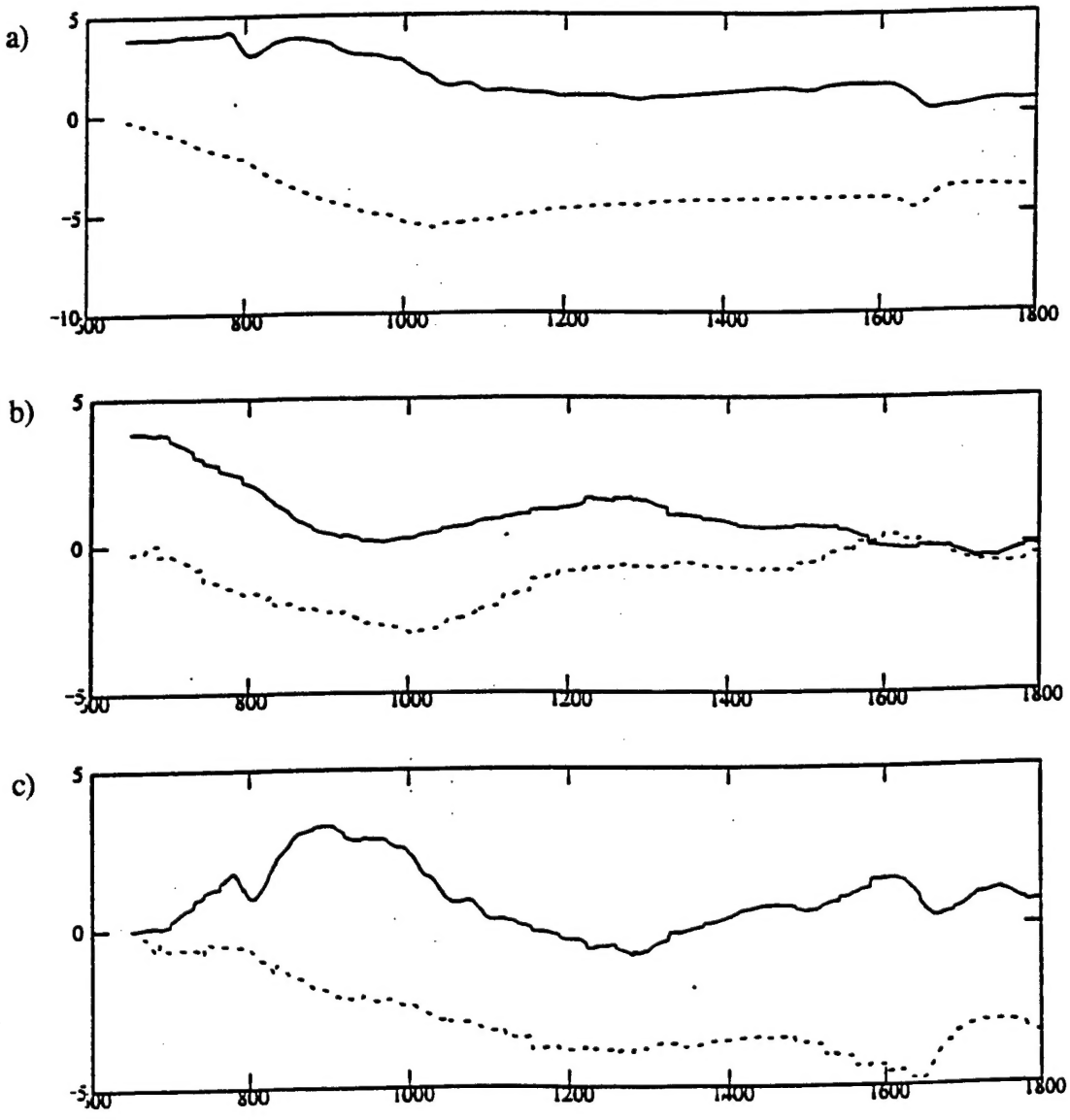

Figure 13. a) Estimates of deflection components; b) true deflection components; c) difference between estimates and true deflections. In all cases the solid line represents the north deflection component. Ordinate values in units of arcseconds; abscissa in seconds.

5 Summary and Conclusion

This report describes some practical experiences with the LN93 and LN100 inertial navigation systems in the area of airborne vector gravimetry. No conclusive results from flight test data analyses can be reported this time, but several aspects of such a gravimetry system have been elucidated. The two inertial navigation systems are designated by the manufacturer as medium-to-high accuracy systems, indicating that the measurements are of sufficient quality that when combined with geodetic quality GPS receivers they should be capable of providing the precision needed to predict the gravity vector with several mgal precision (not accuracy, because of long-term drifts in the gyro data). The two systems under this discussion have significantly different data output capabilities. In each case special data processing algorithms must be developed to make optimum use of the data. These algorithms are described in detail in Section 3. They differentiate between the type of output, whether precise velocities and direction cosines (LN93) or raw accelerometer and gyro data (LN100), and the type of methodology used to combine the INS and GPS data, whether by time-integrating the INS data or by time-differentiating the GPS data.

Each of these possible processing algorithms carries its own advantages and disadvantages. Using the velocities determined by the INS navigation computer may provide the best available INS velocities, since they are based on the manufacturer's (in this case Litton's) extensively tested navigation algorithm. Using the raw accelerometer data yields more flexibility in applying different methodologies to combine the INS and GPS data, for example, allowing them to be more tightly coupled. Using a Kalman filter to estimate the gravity disturbance components from time-integrated IMU data is founded on optimal estimation theory, but requires a stochastic model for the gravity disturbance. Also, the vertical component cannot be estimated since the IMU data are not stable when integrated in the vertical dimension. Using a straightforward differencing of IMU and time-differentiated GPS accelerations to obtain the gravity disturbance vector is a natural extension of the quite successful airborne (scalar) gravimetry concept. However, a unified approach that optimally accounts for IMU errors has yet to be developed and tested.

Several system tests were conducted in the laboratory and in the field to determine the quality of the INS and to begin testing the algorithms for vector gravimetry. These tests showed that the INS's are performing as expected. However, several complications in physical system integration and limited availability of suitable test data have precluded extensive analysis of these algorithms at this time. It is anticipated that continued development of data processing methodologies and more application-specific airborne testing will bear fruit in these areas. The simulation studies conducted by numerous authors and the limited test results shown here all point in that direction.

6 Acknowledgments

The work described in this report was supported by a research project funded by the National Imagery and Mapping Agency (NIMA) and administered by the U.S. Air Force Phillips Laboratory under contract no. F19628-95-K-0020, OSU Research Foundation project no.731618.

7 References

Balmino, G. and F. Sanso (eds.) (1995): New geoids in the world. Bulletin d'Information no.77, Bureau Gravimetrique International; International Geoid Service, Bulletin no.4, Milano, Italy.

Britting, K.R. (1971): *Inertial Navigation Systems Analysis*. John Wiley & Sons, Inc., New York.

Brozena, J.M. and M.F. Peters (1994): Airborne gravity measurement at NRL. Proc. Internat. Symp. on Kinematic Systems in Geodesy, Geomatics and Navigation (KIS94), Banff, Alberta, 30 August - 2 September 1994, pp.495-506.

Grejner-Brzezinska, D. and B. Phuyal (1998): Positioning accuracy of the Airborne Integrated Mapping System. Submitted to *Journal to Geodesy*.

Eissfeller, B. and P. Spietz (1989): Basic Filter Concepts for the Integration of GPS and an Inertial Ring Laser Gyro Strapdown System. *Manus. Geodaetica*, **14**, 166-182.

Forsberg, R. and S. Kenyon (1994): Evaluation and downward continuation of airborne gravity data - the Greenland example. Proc. Internat. Symp. on Kinematic Systems in Geodesy, Geomatics and Navigation (KIS94), Banff, Alberta, 30 August - 2 September 1994, pp.531-538.

Gleason, D.M. (1992): Extracting Gravity Vectors from the Integration of Global Positioning System and Inertial Navigation System Data, *J. Geophys. Res.*, **97**(B6), 8853-8864.

Heiskanen W.A. and H. Moritz (1967): *Physical Geodesy*, W.H. Freeman, San Francisco.

Helmert, F.R. (1880): *Die Mathematischen und Physikalischen Theorien der höheren Geodäsie*. Teubner, Leipzig.

Humphrey, I. and T. Kawakami (1996): User Friendly Bus Controller GPS/INS Integration Software Documentation. Interim Report for USAF Phillips Laboratory, Contract F19628-91-C-0127; prepared by Mayflower Communications, Inc.

Jekeli, C. (1988): The Gravity Gradiometer Survey System (GGSS). *EOS, Trans. Am. Geophys. Union*, **69**, 105ff.

Jekeli, C. (1993): A review of gravity gradiometer survey system data analysis. *Geophysics*, **58**(4), 508-514.

Jekeli, C. (1995): Airborne vector gravimetry using precise, position-aided inertial measurement units. *Bulletin Géodésique*, **69**(1):1-11.

Jekeli, C. (1997) The effect of Earth's gravity field on precise, 3-D free-inertial navigation. *Navigation*, **44**(3), 347-357.

Jekeli, C. (1998a): An analysis of vertical deflections derived from high-degree spherical harmonic models. submitted to *Journal of Geodesy*.

Jekeli, C. (1998b): *Inertial Navigation Systems with Applications in Geodesy.* Textbook in preparation (lecture notes for OSU course GS745, Inertial Navigation/Positioning Analysis).

Jekeli, C. and R. Garcia (1997): GPS phase accelerations for moving-base vector gravimetry. *Journal of Geodesy*, 71(10), 630-639.

Lemoine, F.G. et al. (1996): The development of the NASA GSFC and NIMA Joint Geopotential Model. Proc. International Symposium on Gravity, Geoid, and Marine Geodesy (GRAGEOMAR 1996), University of Tokyo, Tokyo, Japan, 30 September - 5 October, 1996.

Milbert, D.G. (1997): An accuracy assessment of the GEOID96 geoid height model for the state of Ohio. Unnumbered report, Feb. 1997, Geodetic Services Division, National Geodetic Survey, NOAA, Silver Spring, Maryland.

Nerem, R.S. (1995): Terrestrial and planetary gravity fields. *Reviews of Geophysics*, **33** supplement.

Nerem, R.S., Jekeli, C., and W.M. Kaula (1995): Gravity Field Determination and Characteristics: Retrospective and Prospective. *Journal of Geophysical Research*, 100(B8), 15,053-15,074.

NIMA (National Imagery and Mapping Agency), Department of Defense World Geodetic System 1984, Third Edition, Technical Report TR8350.2, NSN 7643-01-402-0347, Bethesda, MD, 1997.

Northrop Corporation, Electronics Division (1986): Gravity Compensation for INS Demonstration Program, Volume 4 - Operational Testing, Report No. AFWAL TR-85-1156, AF Wright Aeronautical Laboratories, Wright-Patterson AFB, Ohio.

Rapp, R.H. (1996): Global models for the 1 cm geoid, present status and future prospects. International Summer School of Theoretical Geodesy, Como, Italy, 26 May - 7 June 1996.

Rose, R.C. and R.A. Nash (1972): Direct Recovery of Deflections of the Vertical Using an Inertial Navigator, *IEEE Trans. Geoscience Electronics*, **GE-10**(2), 85-92.

Schwarz, K.P., O. Colombo, G. Hein, and E.T. Knickmeyer (1992): Requirements for Airborne Vector Gravimetry, in Proc. IAG Symp., From Mars to Greenland: Charting Gravity with Space and Airborne Instruments, General Assembly of the IUGG, Vienna, 1991, Springer Verlag, New York, pp.273-283.

Schwarz, K.P., Z. Li (1996): An introduction to airborne gravimetry and its boundary value problems. International Summer School of Theoretical Geodesy, Como, 26 May - 7 June 1996.

Wang, J., F. Dwaik, and C. Jekeli (1997): INS, GPS, and photogrammetry integration for vector gravimetry. Proc. Internat. Symp. on Kinematic Systems in Geodesy, Geomatics and Navigation (KIS97), Banff, Alberta, 3-6 June 1997, pp.571-579.